Scheduled for publication in the November 1999 issue of The Astronomical Journal.

Spectroscopic Classification of Late-M and L Field Dwarfs

Eduardo L. Martín

Astronomy Department, University of California, Berkeley, CA 94720, USA, ege@popsicle.berkeley.edu

Xavier Delfosse

Instituto de Astrofísica de Canarias, 38200 La Laguna, Spain, delfosse@ll.iac.es

Gibor Basri

Astronomy Department, University of California, Berkeley, CA 94720, USA, basri@soleil.berkeley.edu

Bertrand Goldman

CEA, DSM, DAPNIA, Centre d'Etudes de Saclay, 91191 Gif-sur-Yvette Cedex, France, bgoldman@hep.saclay.cea.fr

Thierry Forveille

Observatoire de Grenoble, 414 rue de la Piscine, Domaine Universitaire de Saint Martin de Hères, F-38041 Grenoble, France, Thierry.Forveille@obs.ujf-grenoble.fr

Maria Rosa Zapatero Osorio

Instituto de Astrofísica de Canarias, 38200 La Laguna, Spain, mosorio@ll.iac.es

ABSTRACT

We present spectra for 12 new ultracool dwarfs found in the DENIS infrared survey. Seven of them have spectral types at the bottom of the M-class (M8–M9.5), and the other five belong to the cooler "L" class. We also present spectra for the two new L dwarfs found by the EROS 2 proper motion survey (Goldman et al. 1999). We introduce a scheme for L dwarf classification that is based on an extension to cooler spectra of a pseudo-continuum ratio previously defined for M dwarfs (Martín et al. 1996). For calibrating the spectral subclasses, we use a temperature scale for late M and L dwarfs obtained from synthetic spectrum fitting of high-resolution profiles of Cs I and Rb I resonance lines (Basri et al. 1999). We define that the subclass range from L0 to L6 corresponds to the temperature range from 2200 K to 1600 K. Our subclasses L0, L1 and L2 agree with Kirkpatrick et al. (1999) but then diverge such that our L6 = L8 (Kirkpatrick).

We find that late-M and L dwarf subclasses can be assigned either in the optical with the PC3 index or in the near-infrared with the H_2O H-band index. We discuss the main photospheric features present in L dwarf spectra, in particular in the region 400–650 nm which has never been shown before. The TiO bands at 549.7, 559.7, 615.9 and 638.4 nm fade with decreasing temperature, but do not vanish until well inside the L domain (∼L5). The Na I 589.0, 589.6 nm resonance doublet in our latest object (L6) becomes the broadest atomic feature ever seen in any cool dwarf. We do not detect H_α emission in our L dwarfs later than L3. We discuss the ages and masses of our objects using their temperatures and absence or presence of lithium. Finally, we compare two L1 dwarfs with different gravities (one with lithium and one without it) and discuss differences in spectral features.

Subject headings: — stars: low-mass, brown dwarfs — stars: evolution — stars: fundamental parameters

1. Introduction

For almost a century astronomers have used the Harvard Spectral Classification Scheme (HSCS; e.g. Cannon & Pickering 1912), which uses the well-known seven letters O, B, A, F, G, K, M. More letters have been added to characterize giant stars with peculiar abundances (C, R, N and S), white dwarfs (D), novae (Q) and Wolf-Rayet stars (W). With the advent of large scale infrared surveys (DENIS, 2MASS), a class of dwarfs cooler than M is beginning to be revealed. The letter L has been proposed to be added to the HSCS in order to characterize them (Martín et al. 1997, hereafter M97). The main reason to chose L was that it is the closest letter to M that is available (N is used for carbon stars). Three L dwarfs have been discovered as companions to stars (Becklin & Zuckerman 1988; Rebolo et al. 1998; Goldman et al. 1999, hereafter G99), but the bulk of the known L dwarfs are free-floating. In a proper motion survey, Ruiz et al. (1997) found the first L dwarf to pass the lithium test (Rebolo et al. 1992; Basri 1998), implying that it is a substellar object. The DENIS survey provided the discovery of the next three field L dwarfs in an area of 230 deg^2 (Delfosse et al. 1997, 1999). One of them was confirmed as a brown dwarf (BD) by the detection of lithium (M97; Tinney et al. 1997, hereafter T97). The fifth free-floating L dwarf, and first in an open cluster, was discovered in a deep CCD survey of the Pleiades (Martín et al. 1998; Zapatero Osorio et al. 1999). Recently, the analysis of 371 deg^2 of the 2MASS survey has given 66 candidate very cool dwarfs, of which 18 have been reported to have spectra consistent with L dwarf classification (Kirkpatrick et al. 1999, hereafter K99).

We present spectroscopic observations of 12 candidate very cool dwarfs discovered by DENIS. Five of them are classified as new L dwarfs. We have also observed 11 L dwarfs that had been previously discovered. The spectral characteristics of our sample of 16 L dwarfs are discussed, and we provide a quantitative method for classifying them based on the slope of the pseudo-continuum in the optical spectra. Our definition of L subclasses uses a temperature scale derived from model fitting of high-resolution spectra (Basri et al. 1999, hereafter B99).

2. Target Selection and Observations

2.1. Selection of DENIS Objects

The new very cool DENIS objects presented in this paper are part of a large sample of DENIS BD candidates which is being selected for statistical and physical study. This selection uses a preliminary version of the DENIS processing pipeline. Delfosse et al. (1999) used custom software for source extraction and photometry. The details of the selection process will be described in a forthcoming paper, and we therefore only summarize it here.

DENIS observations are carried out on the ESO 1 m telescope at La Silla (Chile), with a three channel infrared camera (Epchtein et al. 1997; Copet et al. 1999). Dichroic beam splitters separate the channels, and focal reducing optics provides image scales of 3" on the 256×256 NICMOS3 arrays used for J and K channels and 1" on the 1024×1024 Tektronix CCD detector of the I channel. The instantaneous field of view is 12' for all three channels, and a focal plane microscanning mirror is used to obtain 1" sampling for the two infrared channels. The sky is scanned in a step and stare mode, along 30 degrees strips at constant right ascension which constitute the basic DENIS observing units.

The image data were processed at the Paris processing center (PDAC) with the standard pipeline software (Borsenberger 1997). The instrumental and sky background are derived from a local clipped mean along the strip. Flat-field corrections are derived from observation of the sunrise sky, which are analysed by a linear regression of the pixel values on the mean background level of each image. Source detection and photometry were performed in the Leiden processing center (LDAC) using a preliminary version of the pipeline, which is derived from the SExtractor package (Bertin & Arnouts 1996). Astrometry is refered to the GSC catalog and is normally accurate to

$\sim$0.6". Photometry is measured through apertures of 7" and 15" radii, plus an automatic adaptive aperture (used in this work). It is to be noted that this is not the final DENIS pipeline, as some improvements are underway for both photometry and astrometry (including the addition of PSF fitting photometry for point sources).

As L dwarfs are a very low fraction of the total DENIS detections, it is essential that the selection scheme has a very low false alarm rate, since even a small "blue leak" would still produce a sample dominated by G and K dwarfs. Some artifact flagging is available in the LDAC catalogs, but its efficiency is still not perfect. We therefore use morphological parameters and the consistency of the photometry through the different apertures to reject additional artifacts, as will be described in detail in a future paper. These criteria together only reject a very small fraction ($\sim$ 1%) of the sources in the catalog, and therefore do not significantly affect its completeness. A final eye screening of L dwarf candidates is on the other hand still needed to reject a small fraction of surviving artifacts.

Candidates are selected on a red $I-J$ colour. We select all objects with a measured $I-J > 2.8$ (later than M7-M8), as well as "I band dropouts", which would be detected at J and K though not at I. The later criterion is tuned towards detected free floating equivalents of Gl 229 B out to $\sim$5 pc, but has identified none to date. As of May 1999 we have analysed $\sim$ 1000 square degrees of DENIS data, from which the objects presented here were culled based on a loosely defined combination of redness and observability. This subsample should therefore not be used for statistical purposes. The new DENIS objects presented in this paper are listed in Table 1, and finding charts are provided in Fig. 1.

2.2. Selection of Other Ultracool Dwarfs

The EROS collaboration initiated in 1996 a proper motion survey, covering $\sim$ 400 deg^2 in two bands, with sensitivities down to V 21.5 and I 20.5. Although the primary aim of the survey is to detect dark halo stars in the Solar neighborhood, it was possible to find LHS102B (because of its high speed and intrinsic faintness) through a preliminary analysis using the first two epochs of the survey (see G99 for details). It was also possible to select the slower object EROS J0032-4405 through its color only. Both objects were confirmed as L dwarfs by DENIS photometry.

The sample of this study also includes ultracool dwarfs discovered by the DENIS mini-survey (Delfosse et al. 1999), and the known BDs Kelu 1 (Ruiz et al. 1997), G-196-3 B (Rebolo et al. 1998) and 2MASSs J0850+1057 (K99), plus a few well known very late M dwarfs.

2.3. Spectroscopic Observations

The spectra were collected in three observing runs with the Keck II Low Resolution Imaging Spectrograph (LRIS; Oke et al. 1995), and one run with the 4 m telescope at Kitt Peak National Observatory (KPNO), using the Cryogenic Camera (Cryocam) spectrograph. The observing log is given in Table 2. At Keck, we rotated the slit in order to be at parallactic angle at the beginning of the exposure in order to minimize refraction losses. This procedure was not done by the observers at KPNO. Weather conditions were good although with scattered cirrus. The nights were not photometric.

All the CCD frames were bias subtracted, flat fielded, sky subtracted, and variance extracted using routines within IRAF[1]. We calibrated in wavelength using the emission spectrum of HgNeAr lamps. Correction for instrumental response was made using spectra obtained in the same night of flux standards with fluxes available in the IRAF environment. We did not use order-blocking filters for the Keck observations of ultracool dwarfs. These objects are so red that second-order contamination is negligible. We observed VB10 without filter and with the OG570 order-blocking filter. We did not find any significant contamination due to second-order light. We observed the flux standard BD+262606 for calibrating the Keck spectra. The standard spectrum obtained without filter was used blueward of 680 nm. The standard spectrum obtained with the OG570 filter was used redward of 680 nm.

A representative selection of our sample[2] is shown in Fig. 2. The red part of the spectrum ($\lambda \geq$900 nm) of some objects is affected by interference fringing in the CCD detector that was not completely removed with the flat field. The effect was worse for objects with low S/N ratio or observed at high inclination angle of the telescope. This problem is clearly visible in the spectra of DENIS-P J0205-1159, LHS 102 B, and EROS-MP J0032-4405 in Fig. 2.

3. Late-M and L Spectral Types

3.1. Definition of Spectral Subclasses

It is now well established (M97, T97, K99) that the spectra of the coolest known field dwarfs is very different from the spectra of the very late M dwarfs. In particular molecular bands of TiO and VO, which are prominent in M dwarfs, but were known to become weaker in LHS 2924 (dM9, Probst & Liebert 1983), fade due to the condensation of Ti and V to dust. These ultracool dwarfs cannot be classified within the M spectral type and a new class must be created. M97 proposed the L class and a first proposal at defining the L subclasses has been made by K99. The latter authors

[1] IRAF is distributed by National Optical Astronomy Observatory, which is operated by the Association of Universities for Research in Astronomy, Inc., under contract with the National Science Foundation.

[2] The reduced spectra are available from E.L. Martín upon request. We plan to make them publicly available.

fill the subclasses down to L8 with the current set of objects.

The T_{eff} scale of the K99 subclasses was based on a qualitative comparison with thermochemical equilibrium calculations by Burrows & Sharp (1999), which have been questioned more recently by Lodders (1999). The T_{eff} scale of our new proposed subclasses is based on spectrum synthesis of high resolution profiles (B99). This scale makes it clear that the current set of objects spans a substantially shorter temperature range than is typical for an HSCS spectral class. We also feel that the differences between some K99 subclasses are too subtle.

We define broader L subclasses that make objects of different subclass easier to distinguish. We caution that using particular spectral features for defining the subclasses can be misleading, for example the ratio of TiO over CrH, because these bands are sensitive to gravity (Section 7) and metallicity. We propose a quantitative spectral classification based on the slope of the pseudo-continuum, using one index that increases monotonically from early M dwarfs to late L dwarfs.

Optical low-resolution spectra of some DENIS objects have already been presented by T97 and Tinney et al. (1998). They identified the main spectral features in the range 600–900 nm. They also measured one of the pseudo-continuum spectral ratios (hereafter PC) defined by Martín et al (1996), namely PC3, and found that it increases for cooler objects. We have also used the PC3 ratio, and we have tried to define a new ratio (PC6) with a broader wavelength baseline. The integration limits for these ratios are given in Table 3 and are shown in Fig. 2. Note that we have slightly broadened the limits of the PC3 ratio with respect to the definition given by Martín et al. (1996). This was done because the current dataset has lower spectral resolution. PC6 turned out to be a less reliable indicator of spectral type than PC3 (Fig. 3). Thus, we adopted PC3 as our primary index for spectral typing. One advantage of PC3 is that it covers a relatively narrow wavelength range, making it rather insensitive to problems with the flux calibration of low-resolution spectra. For the dwarfs that have spectra coming from different telescopes, we find that the scatter in PC3 values implies typical uncertainties smaller than 0.5 subclass. We supplemented our data with M dwarf spectra available over the World Wide Web from the references given in Table 4.

The recipe to derive M and L spectral subclasses using the PC3 index can be divided in two spectral ranges. For spectral types between M2.5 and L1, we find the following relationship:

$$SpT = -6.685 + 11.715 \times (PC3) - 2.024 \times (PC3)^2$$

and for spectral types from L1 to L6, we obtain:

$$SpT = 8.557 + 1.181 \times (PC3) - 0.047 \times (PC3)^2$$

where SpT is the spectral subtype (numbers $\geq$10 correspond to L-types, eg. 14 = L4). The standard deviation (1σ) of these polynomial fits to the data given in Table 4 are 0.28 subclasses and 0.54 subclasses, respectively. The slope of PC3 with respect to subclass is steeper for the late L dwarfs because the region at 754.0–758.0 nm is affected by the blue wing of the broad K I resonance doublet.

Our calibration of the PC3 index establishes a quantitative way to determine spectral types with an uncertainty ±0.5 subclasses. We find spectral subclasses that are consistent with those found in the literature for the same objects within 0.5 subclasses (consistent with the general uncertainty in the subtypes), with the exception of the latest L dwarfs. Our coolest L subtypes (L4–L6) are systematically earlier by 1 or 2 subtypes than those of K99 for the objects in common. The relationship of K99 subclasses to our subclasses is as follows: L0, L1 and L2 are the same, $L3_{K99}$=L2.5, $L4_{K99}$=L3, $L5_{K99}$=L4, $L6_{K99}$=L5, $L7_{K99}$=L5.5, $L8_{K99}$=L6. These conversions should be accurate within 0.5 subclasses. We are planning to observe all the K99 L dwarfs in order to improve the conversion, and to check for variability.

Our choice of L subtypes has been informed by the temperatures derived by B99 from synthetic spectrum fitting of the profiles of the Rb I 794.8 nm line and the Cs I 852.1 nm line observed at high resolution. They used model atmospheres that include the formation and condensation of dust grains. The T_{eff} values adopted by B99 for the objects in common with our low-resolution observations are given in Table 5. The borderline between M and L dwarfs is located at T_{eff} ∼2200 K. This is consistent with the estimate made by Martín et al. (1998) using the Pleiades BD sequence. The coolest DENIS L dwarf (DENIS-P J0255-4700) has T_{eff}=1600 K. We find that the coolest 2MASS dwarf reported by K99 (2MASSW J1632+1904) has similar spectral type, although it appears to be slightly cooler because it has a larger PC3 index (Table 4). Hence, the range of T_{eff} covered by our sample of L dwarfs is 600 K. Although the absolute scale of temperatures may change with more refined model atmospheres, or by looking at different parts of the spectrum, the relative scale is likely to be more robust. We note that there is a trend to find lower T_{eff} from model fitting to broad-band photometry or low-resolution infrared spectra (G99; Leggett et al. 1998: Ruiz et al. 1997) than from fitting high-resolution line profiles (B99).

We introduce a division of the L spectral subclasses with a constant T_{eff} step of 100 K. The main justification of this approach is that a spectral scale of subclasses is a proxy for a temperature scale, so it makes sense to follow systematically the guidance of the T_{eff} scale derived by B99. A spectral classification based on detailed spectral features is subject to the effects of gravity and metallicity on those features. It is also dependent on the spectral resolution and S/N ratio of the spectra. We favor a classification scheme based on a PC index that should be relatively insensitive to those problems. Our L subclasses are still preliminary because of several problems: 1) We still lack examples of objects that show the onset of methane formation. The difference in T_{eff} between the coolest L dwarf known and Gl 229 B is about 600 K. 2) We need repeated observations of L dwarfs that can be used as standards. We know almost nothing about the variability (weather?) of these objects. 3) The model atmospheres are still being developed.

For extending the spectral classification to cooler objects, in particular to Gl 229 B (T_{eff}=900 K; Leggett et al. 1999) and the new free-floating methane dwarfs (Strauss et al. 1999; Burgasser et al.

1999), a constant step of 100 K would imply that the end of the L class is at ∼1200 K, which roughly coincides with the expected appearance of strong methane in the K-band spectrum[3]. A new class with a different letter could be used at T_{eff} <1200 K because of the appearance of strong methane bands in the near-IR (H and K bands) spectrum. We suggest that the letter "H" is preferable to "T" (proposed by K99) because the latter one could lead to incorrect association with T Tauri stars and T-associations. Furthermore, H is within the range of letters of the current HSCS (from A to M).

3.2. Spectral Subclasses Versus Infrared Colors and Infrared Spectral Indices

In Fig. 4 we plot our L subclasses versus I-J and I-K colors for dwarfs M8 and later. Both of them tend to increase for cooler objects as expected, but I-K seems to saturate around L4. However, there are not enough objects and the measurement error bars are too large for making a strong conclusion.

We note that the I-K color of the coolest BD known (Gl 229 B) is 5.6 (Matthews et al. 1996), which is identical to that of LHS 102 B (G99). Thus, it seems that the I-K color is not a good indicator of temperature for ultracool dwarfs. This behaviour may be due to strong absorption of H_2O and H_2 in the K-band spectrum of late L dwarfs (Tokunaga & Kobayashi 1999) and methane in Gl 229 B (Oppenheimer et al. 1995). On the other hand, Gl 229 B has I-J=5.8, which is significantly larger than our L dwarfs, so this color may be a good indicator of temperature for ultracool dwarfs although with considerable scatter as shown if Figure 4.

Delfosse et al. (1999) presented low-resolution (R=440) infrared spectroscopic observations of some DENIS VLM stars and BDs. They measured H_2O and CO indices that are expected to be sensitive to T_{eff} and gravity (Jones et al. 1994). In order to test if there is a good correspondance between these indices and our spectral types derived from optical spectra, we have plotted the index values given by Delfosse et al. versus our subclasses (Figure 5). We confirm that the H_2O H-band index is very sensitive to temperature. The H_2O K-band index is not temperature sensitive as noted by Tokunaga & Kobayashi (1999). The CO index is somewhat sensitive to T_{eff}, although less that the H_2O H-band index. CO was used by Delfosse et al. (1999) as a gravity indicator. The good correlation between the H_2O H-band index and our optical subclasses indicates that L subclasses can be obtained from near-infrared spectra using the following linear relationship:

$$SpT = 2.428 + 1.9855 \times (H_2O_{H-band})$$

$$1\sigma = 0.31 \text{ subclasses}, \text{Range} = M9.5 - L5.0$$

---

[3]Noll et al. 1999 have noted that methane could appear in the L-band spectrum at T_{eff} ∼1700 K)

where H_2O_{H-band} is the steam H-band index used by Delfosse et al. (1999).

4. Absorption Features

The absence of strong TiO bands in the optical spectrum, and the presence of strong resonance doublets of alkali elements (K I 766.5, 769.9 nm; Rb I 780.0, 794.8 nm; and Cs I 852.1, 894.3 nm) were the first noted characteristics of L dwarfs (Ruiz et al. 1997; M97). Tinney et al. (1998) and K99 have identified the molecular features present in the low-resolution optical spectrum of L dwarfs in the range 675.0–997.0 nm. Our LRIS spectra include the blue optical range up to 355 nm, but the flux blueward of about 410 nm drops below our detection limit and we only have noise. In Figure 6, we present the spectra of our brightest very late M and L dwarfs in the region 410–650 nm. The strength of the Na I 589.0, 589.6 nm resonance doublet increases for cooler $T_{\rm eff}$. The line becomes extremely broad in our coolest L dwarf, and produces a bump at about 500 nm. This is the broadest feature ever seen in any dwarf.

We identify the following TiO bandheads in the blue part of our LRIS spectrum of LHS 2397 a (dM8.5): 476.1, 495.5, 516.7, 524.0, 544.8, 549.7, 559.7, 586.2, 615.9, 638.4 nm. All these bands are well-known in the spectra of late-K and early M stars (Coluzzi 1993). In the spectrum of our brightest dL0 object (DENIS-P J0909-0658) the features blueward of 544.8 nm have dissapeared, but we do see the redder TiO features (Figure 6). The TiO bands at 549.7, 559.7, 615.9 and 638.4 nm persist until ∼L5 subclass. K99 have noted the presence of weak TiO at 843.2 nm in DENIS-P J1228-1547 (bdL4.5), which we also see in our spectra.

In Fig. 7 we show the spectral region around the K I resonance doublet. This feature becomes very broad in the late L spectra, but not as broad as the Na I resonance doublet because K has a lower abundance than Na. The Rb I resonance doublet is also shown in this figure, and it increases in strength toward cooler temperatures. There are TiO and VO bands in this spectral range, which are seen in the late-M and early-L dwarfs, but not in the L6 dwarf. On the other hand, the bandhead of CaH at ∼685 nm is still clearly present in this latter object. In contrast with M dwarfs, it is characteristic of L dwarf spectra that hydride bandheads are as strong or stronger than oxide bandheads. The CrH and FeH bandheads at 861.1 and 869.2 nm are very strong as shown in Figure 8. In the same Figure, we also show that the strength of the Cs I resonance doublet increases with decreasing $T_{\rm eff}$, confirming the results of B99.

In Table 6 we give the strength of several molecular bandheads using the ratios defined in Table 3. In Fig. 9 we plot these ratios against our spectral subclasses. The CrH and FeH have similar behaviour. Both increase with later subclass, until they reach a maximum at L3–L4, and then they decrease sharply for cooler temperatures. Lodders (1999) predicts that CrH and FeH dissapear with the formation of dust grains for a temperature of 1850 K, which is in good agreement with our temperature scale. The TiO molecule increases until M8, where it is at its strongest, and then decreases steadily for cooler L dwarfs. The VO molecule also has a maximum at M8 subclass, but it has a less pronounced decrease than TiO with cooler temperatures. K99 state that the VO bandheads at 740 nm and 790 nm are strongest in L0 dwarfs, but we do not see this in our data. Their VO indices actually have a maximum at M9, which is more consistent with our results.

In Table 7 we give our pseudo-equivalent width (PEW) measurements of H_α, Li I 670.8 nm, Na I 818.3,819.5 nm (which are blended at our low resolution and contaminated with a telluric band), and Cs I 852.1 nm. The behaviour of the latter two features is shown in Figure 10. For Cs I 852.1 nm we plotted both our measurements and those measured in the high-resolution spectra presented by B99. Note that the PEW of Cs I 852.1 nm is systematically higher in the low-resolution spectra. Caution must be excercized when comparing PEW values obtained from spectra of different resolution.

In Fig. 11 we show a zoom of the Li I 670.8 nm region in selected targets. Our PEW (Li I 670.8 nm) are in good agreement with those reported by K99 for 5 objects in common, with the exception of Kelu 1. Our value is PEW=0.6±0.3, their value is PEW=1.7±0.2, Ruiz et al. (1997) reported PEW=1.0±0.05, and Martín et al. (1998) gave 4.3±0.6. The discrepancy among these values is larger than the error bars, suggesting that lithium could be variable in Kelu 1. B99 find high rotation (vsini=80 km/s) for this object, the highest among their sample of 8 L dwarfs. Perhaps lithium is a good indicator of the presence of inhomogeneities in the surface, but B99 do not see variability in four high-resolution spectra obtained on different nights. The L6 dwarf 2MASSW J1632+1904 shows a possible lithium feature with PEW$\sim$7 Å. However, our spectrum is noisy in this spectral region. There is another feature centered at 661 nm that is probably not real and has similar strength than the putative lithium line. All we can say at this point is that our spectrum is suggestive of the presence of lithium, but more data is needed to confirm it.

5. H_α Emission

We measured the PEW of H_α emission by direct integration of the profile using the task splot in IRAF, or we estimated upper limits from the maximum strength of noise fluctuations in the range 655–660 nm. We attempted to measure PEWs in the Keck/LRIS spectra only, because the KPNO data is rather noisy at H_α.

In order to study the behaviour of chromospheric activity as indicated by H_α, we have supplemented our PEWs with values taken from the literature (Basri et al. 1996; K99; Martín et al. 1996; Tinney et al. 1997; Tinney & Reid 1998). For the stars with several measurements, we have rejected any values 3 σ higher than the mean (to avoid flares) and we have averaged the rest. High values were rejected for VB8, LHS 2065, LP 412, BRI 1222 and LHS 2397a. In Fig. 12, we plot H_α PEW versus spectral type. There seems to be a slight trend toward decreasing emission in the L dwarfs. We note that none of the 10 objects cooler than L3 have detected emission, although the upper limits are rather high in some cases. We also note that the L-type confirmed BDs (with lithium) do not have stronger emission than other L dwarfs, even though they are younger than about 1 Gyr (M97).

The ratio of the luminosity in the H_α line to the bolometric luminosity is arguably a better chromospheric diagnostic than the PEW. Tinney & Reid (1998) have provided an H_α bolometric correction for M dwarfs as a function of I-K color. However this color correlates poorly with T_{eff} for L dwarfs, and their bolometric correction cannot thus be extrapolated into the L dwarf regime.

6. Ages and Masses of L Dwarfs

In Fig. 13 we show the temperature versus mass theoretical predictions of the most recent evolutionary models available to us (hereafter referred to as the "Lyon" models). The Nextgen models do not include dust effects (Allard et al. 1997; Chabrier & Baraffe 1997; Baraffe et al. 1998), but the Dusty models do (Allard et al. 1999). The effect of dust is modest in the T_{eff} of the evolutionary models, although the colors do change substantially because the atmosphere is quite different. The Lyon models indicate that most L dwarfs are substellar because only for the oldest age (10 Gyr) are the very lowest mass stars expected to cool to ~2000 K. The Dusty models push the substellar mass limit to a slightly lower mass (0.072 $M_\odot$) than the Nextgen models (0.075 $M_\odot$). This is indicated in Fig. 13 with two vertical dotted lines. On the other hand, the models of Burrows et al. (1997) cool to ~1100 K for 0.076 $M_\odot$ at 10 Gyr. Objects with L subclasses later than L1 (2000 K) have substellar masses if the Lyon models are correct, but not necessarily so if the Burrows et al. models are correct. We have been conservative in giving certified BD status to our objects. Only the ones that show lithium have been flagged with the prefix "bd" instead of "d" before the spectral subclass, as proposed by M97.

The lithium test was put forward to distinguish between M-type VLM stars and young BDs (Rebolo et al. 1992; Magazzù et al. 1993). It has been successful in doing so in the Pleiades cluster (Basri et al. 1996; Rebolo et al. 1996) and in the field (Ruiz et al. 1997; M97; Tinney et al. 1997; Tinney 1998; Martín et al. 1999). In Fig. 14 we show the prediction for lithium depletion versus mass for the Lyon models. Most L dwarfs are substellar, but only those that are relatively young (age~0.1 Gyr) or less massive than about 0.05 $M_\odot$ have preserved lithium. If we only know the temperature of an L dwarf, we can constrain its age and mass from the absence or presence of lithium in the spectrum (M97). For example, for DENIS-P J1441-0945 (dL1) we do not detect lithium, so it must have a mass larger than 0.05 $M_\odot$ according to Fig. 14. We cannot be sure whether this object is an old VLM star or a contracting BD without further information. On the other hand, EROS-MP J0032-4405 (bdL0.5) has a strong lithium line. If no lithium burning has occurred, the Lyon models indicate that it must be a BD with a mass of $\leq$0.05 $M_\odot$. If the object has partially depleted its initial Li content, the mass would be in the range 0.06–0.05 $M_\odot$. The lack of lithium in the DENIS L6 dwarf could be due to lithium burning and/or the lack of atomic lithium because of formation of LiCl and LiOH (Burrows & Sharp 1999; Lodders 1999). The detection of lithium in the 2MASS L6 dwarf (if confirmed) would imply that the Li resonance line is still strong at ~1600 K, and that the 2MASS object has lower mass than the DENIS object.

We plan to analyze in detail the formation of the lithium resonance line in L dwarfs using synthetic spectra.

The maximum mass of an L dwarf corresponds to its maximum age. For example, if DENIS-P J1441-0945 is 10 Gyr old, it would have a mass (inferred from Fig. 13) of about 0.075 $M_\odot$, but if it is 1 Gyr old, the mass would be lower (0.070 $M_\odot$). Both combinations are consistent with total lithium depletion. The age of EROS-MP J0032-4405 is constrained by the presence of lithium because BDs with masses $\leq$0.05 $M_\odot$ and temperatures $\sim$2000 K have to be younger than 0.5 Gyr (Fig. 13). Adding our results to those of K99, we find that out of 31 known L dwarfs, 9 have lithium detections. The L dwarfs with lithium are less massive than those without it. The result that about 70% of the L dwarfs do not have lithium is most likely due to the sensitivity limits of the DENIS and 2MASS surveys. The search volume for more massive BDs is larger than for less massive ones. We postpone for a future paper a discussion of the luminosity and mass function of the L dwarfs.

Trigonometric parallaxes were available for only a few L dwarfs at the time of writing this paper, namely: 2MASP J0345432+254023 (28.2±0.65 pc, K99), 2MASSW J1439284+192915 (15.4±0.75 pc, K99), GD 165 B (31.54±2.3 pc, K99), DENIS-P J0205-1159 (16.64±0.8 pc, K99), LHS 102 (9.6±1.2 pc, G99), and Kelu 1 (19±1 pc, C. Dahn private communication, M.T. Ruiz private communication). In Fig. 15 we show a color-magnitude diagram. The photometric data have been taken from Leggett et al. (1998), G99 and K99. The comparison of the data with the Dusty models is not satisfactory for some objects but is much better than with the Nextgen models (which are too blue in J-K).

LHS 102 B (dL4) is the reddest object in J-K among those plotted in Fig. 15. It lies right on the track for 5 Gyr, but the observational error bar allows a large range of ages (Fig. 15). G99 obtained the same age using the Lyon models in a M_I versus I-K diagram. We think that the parallax of this object is probably the most reliable of the 6 L dwarfs plotted in Fig. 15 (although it is not the one with the smaller error bar) because it was obtained from the bright primary LHS 102 A, and because this is the nearest object of the six. LHS 102 B does not show lithium, which is consistent with the 100% lithium depletion predicted by the Lyon models for an age of 5 Gyr and a mass of 0.072 $M_\odot$. The coolest object plotted in this diagram is DENIS-P J0205-1159 (dL5). It is the one that has the faintest M_K as well. It lies below the 10 Gyr isochrone, suggesting that the Dusty models may not be giving the right magnitudes for the J and K filters at this low temperature. On the other hand, the problem could be that the trigonometric parallax is incorrect. GD 165 B also lies slightly below the 10 Gyr isochrone, but the difference is within the error bar. Three objects are located in the region where lithium is expected to be preserved in Fig. 15. Two of them do not have lithium (2MASP J0345432+254023 and 2MASSW J1439284+192915) and one does (Kelu 1). If the parallaxes are correct, the two objects without lithium contradict the Lyon models, and Kelu 1 appears to be surprisingly young (age $<$ 0.1 Gyr). If the models are valid, they suggest that these three L dwarfs might be binaries. No companion to Kelu 1 has been seen in HST/NICMOS images (Martín et al. 1999b). If Kelu 1 is a binary, it must have an orbital separation smaller than about 1.5 AU. It would be interesting to check whether it is a radial velocity variable.

7. Gravity Effects

It is interesting to compare two objects that have the same spectral subclass (L1) but different gravities [4]. DENIS-P J1441-0945 does not have lithium, so it must have a mass larger than 0.05 $M_\odot$ and an age $\geq$0.5 Gyr. G 196-3 B has lithium (Rebolo et al. 1998, confirmed in this work), so it must have a mass lower than 0.05 $M_\odot$ and an age <0.5 Gyr. It is likely that the latter object is quite young because it is a companion of an X-ray active early-M dwarf. We have investigated if there are differences in the spectrum that might be due to the effects of gravity on line formation and/or dust formation and condensation. Both DENIS-P J1441-0945 and G 196-3 B were observed in the same LRIS run with the same instrumental configuration. The spectra are shown in Fig. 16. The slope of the spectra is similar, but there are significant differences in spectral features. The younger and less massive object (G 196-3 B) has lower gravity and presents weaker TiO bands and weaker CrH and FeH bands than the older and more massive object (DENIS-P J1441-0945). Higher gravity seems to favor the formation of these molecular features. We note that spectral subclasses inferred from the comparison of TiO bands with hydride bands (K99) will be affected by gravity effects. The dependance of the PC3 index with gravity also needs to be investigated. This index could be affected by gravity effects on the wings of the K I resonance doublet for very cool dwarfs where this feature is very broad. The VO bands are not weaker in G 196-3 B than in DENIS-P J1441-0945. Martín et al. (1996) found that VO is stronger in the Pleiades M-type BDs than in field dwarfs of the same spectral type. Luhman (1999) reports a stronger difference in VO strength between M8 objects in star-forming regions and field dwarfs. In Fig. 9 we plotted with different symbols the dwarfs with and without lithium detections. The number of dwarfs with lithium is still to small to draw definite conclusions, but there seems to be a trend of weaker molecular features in dwarfs of lower gravity (lithium BDs) than in higher gravity dwarfs, which are older and more massive.

The resonance doublets of Na I and K I are slightly weaker in G 196-3 B than in DENIS-P J1441-0945. The subordinate infrared doublet of Na I is also weaker in G 196-3 B. These gravity effects are similar to those observed in very late M dwarfs (Luhman 1999 and references therein). B99 noted that the Cs I and Rb I lines of G 196-3 B appear too weak for its spectral type. The use of gravity sensitive features may allow a definition of luminosity classes for ultracool objects in the future.

8. Conclusions

Twelve new BD candidates found in the DENIS infrared survey have been presented. We have obtained low resolution spectroscopic observations of these objects and of 9 previously known L dwarfs. We have measured in our spectra the PC3 index originally defined by Martín et al. (1996)

---

[4] We implicitly assume solar metallicity for both objects because they are likely to belong to the disk population

and a new index PC6. We have also measured these indices in spectra of M dwarfs available in the literature. The PC3 index is found to increase monotonically with cooler temperature, but the PC6 index does not. We provide two calibratios of the PC3 index against spectral subclass, one for the range M2.5–L2.0 and another one for the range L2.0–L6.0. We have separated the L subclasses in steps of 100 K according to the temperature scale derived by B99 from synthetic fitting of high-resolution spectra. Our objects span the subclass range L0–L6 which corresponds to a temperature range of 2200 K–1600 K according to the atmosphere models used by B99, which include the effects of dust formation and condensation. Our L subclasses are in good agreement (within 0.5 subclass) with those defined by K99, except for the latest L objects, where the discrepancy is up to two subclasses.

We find that there is a linear relationship between our subclasses and the H_2O H-band spectral index measured by Delfosse et al. (1999), but not with the H_2O K-band index. L subclasses can be assigned either in the optical with the PC3 index or in the near-infrared with the H_2O H-band index. The I-K color seems to saturate around L4 and does not seem to be a good indicator of temperature. The I-J color appears to be a better temperature indicator than I-K for L dwarfs and Gl 229 B.

We discuss the main photospheric features present in L dwarf spectra, in particular in the region 400–650 nm for which we present the first observations. The TiO bands at 549.7, 559.7, 615.9 and 638.4 nm fade with decreasing temperature, but do not subdue completely until well inside the L domain ($\sim$L5). The Na I 589.0, 589.6 nm resonance doublet grows with decreasing temperature. In our latest object (L6), it becomes the broadest feature ever seen in any cool dwarf.

The PEW of H_α emission measured in our spectra have been provided. We find a trend toward decreasing emission in the L dwarfs. None of the 10 objects known to be cooler than L3 have detected emission, although the upper limits are rather high in some cases. Brown dwarfs (bdL, with lithium) do not have stronger emission than other L dwarfs, even though they are younger than about 1 Gyr.

The most recent Lyon models suggest that most L dwarfs are substellar ($M<0.075$ $M_\odot$) but the older models of Burrows et al. (1997) predict cooler temperatures for stars at the bottom of the main-sequence. We have been conservative and have assigned the status of confirmed BD only to the objects that pass the lithium test. Our observations provide the first lithium detection in EROS-MP J0032-4405, confirming it as substellar object with mass $\leq$0.05 $M_\odot$ and age $\sim$0.5 Gyr or younger. We have not found lithium in any of the new DENIS dwarfs. The ratio of L dwarfs with and without lithium is about one third. For a subset of 6 L dwarfs with known parallaxes we have compared the M_K versus J-K color magnitude diagram with the Lyon models. We find good agreement for LHS 102 B (no lithium, 5 Gyr, 0.072 $M_\odot$) and GD 165 B (no lithium, 10 Gyr, 0.073 $M_\odot$). For the other objects there are problems: Kelu 1 appears to be surprisingly young (age<0.1 Gyr). The 2MASS objects appear to be young and should have lithium, but they do not pass the lithium test. GD 165 B and DENIS-P J0205-1159 lie below the isochrone for 10 Gyr.

There seems to be three possible explanations: 1) Uncertainties in the models for young ages ($\sim$100 Myr); 2) Unresolved binaries; 3) Problems with the parallaxes. If Kelu 1 is a binary, it must have a separation smaller than 1.5 AU, and it could be detected with high-precision radial velocity measurements.

Finally, we have made a detailed comparison of the LRIS spectra of two dwarfs of similar spectral type (L1) but different gravities. Due to its strong lithium line and X-ray activity of its primary, G 196-3 B is considered to be a young BD with mass $\leq$0.05 $M_\odot$ and age younger than 0.5 Gyr. On the other hand, DENIS-P J1441-0945 has no lithium so it must have a mass >0.05 $M_\odot$ and an age older than 0.5 Gyr. The main differences in the spectra of these two objects are that the young (lower gravity) BD has weaker TiO and hydride bands than the older dwarf. The features due to Na I and K I are slightly weaker in the young BD.

Acknowledgments: Data presented herein were obtained at the W. M. Keck Observatory, which is operated as a scientific partnership among the California Institute of Technology, the University of California and the National Aeronautics and Space Administration. The Observatory was made possible by the generous finantial support of the W. M. Keck Foundation. We also acknowledge the use of the 4 m telescope at Kitt Peak National Observatory. We have made use of the Simbad database, operated at CDS, Strasbourg, France. We thank the following people: David Ardila, Kevin Luhman and Victor Sánchez Béjar for their cooperation in obtaining spectroscopic data, Subu Mohanty for help with the comparison with the high-resolution spectra, and the Lyon group (France Allard, Isabelle Baraffe, Gilles Chabrier and Peter Hauschildt) for providing models. We are grateful to the PI (Nicolas Epchtein) and the members of the DENIS consortium whose work made these results possible. The DENIS project is partly funded by the European Comission through SCIENCE and Human Capital and Mobility grants. It is also supported in France by INSU, the Education Ministry and CNRS, in Germany by the Land of Baden-Würtenberg, in Spain by DGICYT, in Italy by CNR, in Austria by the Fonds zur Forderung der Wissenshaftlichen Forschung, in Brazil by FAPESP, and in Hungary by an OTKA grant and an ESO C&EE grant. EM acknowledges the support of the Spanish Ministry of Education and Culture. GB acknowledges the support of the National Science Foundation through grant AST96-18439.

REFERENCES

Allard, F., Hauschildt, P. H., Alexander, D. R. & Starrfield, S. 1997, ARAA, 35, 137

Allard, F. 1999, in "Very Low-Mass Stars and Brown Dwarfs in Stellar Clusters and Associations", ed R. Rebolo, M. R. Zapatero Osorio, in press

Basri, G., Marcy, G., & Graham, J. R. 1996, ApJ, 458, 600

Basri, G. 1998, in "Brown Dwarfs and Extrasolar Planets", ed. R. Rebolo, E. L. Martín, M. R. Zapatero Osorio (ASP: San Francisco), p. 394

Basri, G., Mohanty, S., Allard, F., Hauschildt, P., Delfosse, X., Martín, E. L., Forveille, T. & Goldman, B. 1999, ApJ, submitted (B99)

Baraffe, I., Chabrier, G., Allard, F., & Hauschildt, P.H. 1998, A&A, 337, 403

Becklin, E. E. & Zuckerman, B. 1988, Nature, 336, 656

Bertin E. & Arnouts S. 1996, A&AS, 117, 393

Bessell, M. S. 1991, AJ, 101, 662

Borsenberger J., 1997, in Proceedings of the 3rd DENIS Euroconference The impact of large scale near-infrared surveys, F. Garzon, N. Epchtein, A. Omont, W.B. Burton, P. Persi (eds) Kluwer Ac. Publishers, Dordrecht, p. 181

Burgasser, A. J. et al. 1999, ApJ, in press

Burrows, A., Marley, M., Hubbard, W. B., Lunine, J. I., Guillot, T., Saumon, D., Freedman, R., Sudarsky, D. & Sharp, C. 1997, ApJ, 491, 856

Burrows, A. & Sharp, C. 1999, ApJ, 512, 843

Cannon, A. J. & Pickering, E. C. 1912, Annals of the Astronomical Observatory at Harvard College, v. 56, no. 4, Cambridge, Mass.: The Observatory, 1912, p. 66

Coluzzi, R. 1993, Bull. Inf. CDS, 43, 7

Copet E. et al 1999, A&AS, in press

Delfosse, X. et al. 1997, A&A, 327, L25

Delfosse, X., Tinney, C. G., Forveille, T., Epchtein, N., Bonsenberger, J., Fouqué, P., Kimeswenger, S. & Tiphène, D. 1999, A&AS, 135, 41

Epchtein, N. et al. 1997, The Messenger, 87, 27

Goldman, B. et al. 1999, A&A, submitted (G99)

Jones, H. R. A., Longmore, A. J., Jameson, R. F. & Mountain, C. M. 1994, MNRAS, 267, 413

Jones, H. R. A. & Tsuji, T. 1997, ApJ, 480, L39

Kirkpatrick, J. D., Reid, N. I., Liebert, J., Cutri, R. M., Nelson, B. Beichman, C. A., Dahn, C. C., Monet, D. G., Gizis, J. E. & Skrutskie, M. F. 1999, ApJ, 519, 802 (K99)

Kirkpatrick, J. D., Henry, T. J. & McCarthy, D. W. 1991, ApJS, 77, 417

Leggett, S. K., Allard, F. & Hauschildt, P. H. 1998, ApJ, 509, 836

Leggett, S. K., Toomey, D. W., Geballe, T. R. & Brown, R. H. 1999, ApJ, in press

Lodders, K. 1999, ApJ, 519, 793

Luhman, K. L. 1999, ApJ, in press

Magazzù, A., Martín, E. L. & Rebolo, R. 1993, ApJ, 404, L17

Martín, E. L., Basri, G., Delfosse, X., & Forveille, T. 1997, A&A, 327, L29 (M97)

Martín, E. L., Basri, G., Zapatero Osorio, M.R., Rebolo, R. & García López, R.J.. 1998, ApJ, 507, L41

Martín, E. L., Basri, G. & Zapatero Osorio, M.R. 1999, AJ, in press

Martín, E. L., Rebolo, R., & Zapatero Osorio, M. R. 1996, ApJ, 469, 706

Matthews, K., Nakajima, T., Kulkarni, S. R. & Oppenheimer, B. R. 1996, AJ, 112, 1678

Noll, K. et al. 1999, poster presented in the meeting "From Giant Planets to Cool Stars", held in Flastaff, Arizona, June 8–11, 1999.

Oke, J. B. et al. 1995, PASP, 107, 375

Oppenheimer, B., Kulkarni, S. R., Matthews, K. & Nakajima, T. 1995, Science, 270, 1478

Pavlenko, Ya. V. 1997, Astronomy Reports, 41, 537

Pavlenko, Ya. V., Rebolo, R., Martín, E. L. & García López, R. 1995, A&A, 303, 807

Probst, R. G. & Liebert, J. 1983, ApJ, 274, 245

Rebolo, R., Martín, E. L., Basri, G., Marcy, G. W., & Zapatero Osorio, M. R. 1996, ApJ, 469, L53

Rebolo, R., Martín, E. L. & Magazzù, A. 1992, ApJ, 389, L83

Rebolo, R., Zapatero Osorio, M. R., Madruga, S., Bejar, V. J. S., Arribas, S. & Licandro, J. 1998, Science, 282, 1309

Ruiz, M. T., Leggett, S.K., & Allard, F. 1997, ApJ, 491, L107

Schweitzer, A., Hauschildt, P. H., Allard, F. & Basri, G. 1996, MNRAS, 283, 821

Silva, D. R. & Cornell, M. E. 1992, ApJS, 81, 865

Strauss, M. A. et al. 1999, ApJ, in press

Tokunaga, A. T. & Kobayashi, N. 1999, AJ, 117, 1010

Torres-Dodgen, A. V. & Weaver, W. B. 1993, PASP, 105, 693

Tinney, C. G. 1998, MNRAS, 296, L42

Tinney, C. G., Delfosse, X. & Forveille, T. 1997, ApJ, 490, L95 (T97)

Tinney, C. G., Delfosse, X., Forveille, T. & Allard, F. 1998, A&A, 338, 1066

Tinney, C. G. & Reid, N. 1998, MNRAS, 301, 1031

Zapatero Osorio, M. R. et al. 1999, A&AS, 134, 537

Fig. 1.— Finding charts obtained with the I DENIS image. The size of this chart is $\sim 3.5' \times 3.5$. North is up and East is left.

Fig. 2.— A representative subset of our Keck spectra in the region 460–1050 nm. They have been normalized to the counts at 750 nm, and shifted with a constant. The flux limits for the PC3 and PC6 indices are shown in the upper right corner.

Fig. 3.— The PC3 index is a better indicator of spectral subclass than the PC6 index. X-axis values larger than 9.5 correspond to L subclasses, i.e., x=10=L0. The uncertainties in the PC indices are smaller than the size of the points.

Fig. 4.— The I-J color increases toward later spectral types in the range M8-L6. The I-K color also increases but seems to saturate at ∼L4.

Fig. 5.— The H_2O "H" (1.51–1.57 μm) and "K" (2.08–2.16 μm) indices and the CO index measured by Delfosse et al. 1999 in low-resolution infrared spectra versus our spectral subclasses. The H_2O "H" index is well correlated with subclass, and can be used to assign spectral types in the infrared.

Fig. 6.— The blue region of our LRIS spectra contains the Na I 589.0, 589.6 nm resonance doublet and several TiO bandheads. Note the weakening of TiO and the strengthening of Na I with later spectral subclass.

Fig. 7.— A zoom of Keck LRIS spectra in the region 670–810 nm. The spectra have been normalized to the counts at 750 nm. Upper panel: Kelu 1 (solid line), EROS-MP J0032-4405 (dotted line); LHS 2065 (dashed line). Lower panel: DENIS-P J0255-4700 (solid line), DENIS-P J1228-1547 (dotted line) and DENIS-P J1058-1548 (dashed line). The main photospheric features are identified in the upper part of each panel, and telluric features are labelled in the lower part.

Fig. 8.— A zoom of Keck LRIS spectra in the region 800–920 nm. The spectra have been normalized to the counts at 750 nm. From top to bottom the objects are DENIS-P J0255-4700 (dL6), DENIS-P J0205-1159 (dL5), DENIS-P J1228-1547 (bdL4.5) and DENIS-P J1058-1548 (dL2.5). The main photospheric features are identified in the upper part, and telluric features are labelled in the lower part.

Fig. 9.— The sum of the CrH (upper left), FeH (upper right), TiO (lower right), and VO (lower left) indices measured by us plotted against our spectral subclasses. Six pointed stars denote dwarfs with no lithium detections. Open hexagons denote dwarfs with lithium detections.

Fig. 10.— Our PEW values for the Na I subordinate doublet (upper panel) and Cs I resonance doublet (lower panel) versus spectral subclass. The empty symbols denote the PEW values of B99 obtained from high-resolution spectra.

Fig. 11.— A zoom of the Li I region of selected objects. The position of the lithium resonance line is indicated with a dotted line.

Fig. 12.— The PEW of H_α declines toward late L types. Six pointed stars denote objects with measured H_α, empty hexagons are lithium BDs with measured H_α, and filled inverted triangles are upper limits.

Fig. 13.— "Lyon model" isochrones in a $T_{\rm eff}$ versus mass plane. Solid lines are Nextgen models and dashed lines are Dusty models. The substellar limit for solar metallicity is at 0.075 $M_\odot$ for Nextgen or 0.072 $M_\odot$ for Dusty (vertical dotted lines). L dwarfs are cooler than 2200 K (horizontal dotted line). H dwarfs start at $T_{\rm eff}$ cooler than 1200 K.

Fig. 14.— "Lyon model" curves of lithium fraction versus mass. The lithium fraction is defined as the ratio of the number of Li atoms at a given time over the initial number of Li atoms. Solid lines are Nextgen models and dashed lines are Dusty models. The curves for ages older than 0.5 Gyr overlap.

Fig. 15.— Color-magnitude diagram with the predictions of the Dusty "Lyon models'. The Nextgen models give unrealistic blue colors and are not shown. The dotted line divides the region where lithium is destroyed by more than 90% (left part of the plot) from the region where it is preserved (right part). The six L dwarfs of known distances are plotted. Empty squares denote objects without lithium. One filled hexagon denotes the object with lithium (Kelu 1).

Fig. 16.— Comparison of the LRIS spectra of two dwarfs of similar spectral type (L1) but different gravities. Note the differences in spectral features. Both objects have been normalized at 750 nm. A boxcar smoothing of 3 points has been applied.

Table 1. New DENIS Ultracool Candidates

Full Name	Position	I	$I-J$	$I-K$
DENIS-P J0243-5432	02:43:51.0 -54:32:19	17.60	3.47±0.12	4.67±0.10
DENIS-P J0255-4700	02:55:03.3 -47:00:49	17.14	3.66±0.10	5.28±0.10
DENIS-P J1023-1336	10:23:04.8 -13:36:08	17.60	2.98±0.17	4.65±0.22
DENIS-P J1024-0719	10:24:20.8 -07:19:11	18.00	2.80±0.16	4.65±0.23
DENIS-P J1047-1815	10:47:31.1 -18:15:58	17.75	3.51±0.10	4.87±0.30
DENIS-P J1116-1945	11:16:20.6 -19:45:46	17.75	2.98±0.10	4.25±0.30
DENIS-P J1158-1201	11:58:28.9 -12:01:57	17.76	2.97±0.13	4.33±0.30
DENIS-P J1159+0057	11:59:38.4 +00:57:27	17.32	3.07±0.12	4.65±0.30
DENIS-P J1208+0149	12:08:31.6 +01:49:24	18.38	2.99±0.18	4.61±0.20
DENIS-P J1323-1806	13:23:35.9 -18:06:38	18.60	3.54±0.25	4.43±0.30
DENIS-P J1431-1953	14:31:01.3 -19:53:49	17.47	2.85±0.12	3.77±0.40
DENIS-P J1441-0945	14:41:37.3 -09:45:59	17.32	3.36±0.12	4.95±0.40

Note. — Equinox J2000, Epoch 1998.

Table 2. Journal of spectroscopic observations

Brief Name	Date	Telescope	Grating	Disp. (Å/pix)	Range (nm)	$\tau_{\rm exp}$ (s)
BRI 0021-0214	1998 Dec 22	KPNO	730	4.20	533.9–959.7	120
	1998 Dec 23	Keck II	150	4.81	355.5–1125.1	600
DENIS-P J0205-1159	1998 Dec 22	Keck II	150	4.81	355.5–1125.1	600
DENIS-P J0243-5432	1998 Dec 23	Keck II	150	4.81	355.5–1125.1	1800
DENIS-P J0247-1055	1998 Dec 22	Keck II	150	4.81	355.5–1125.1	600
DENIS-P J0255-4700	1998 Dec 23	Keck II	150	4.81	355.5–1125.1	1200
DENIS-P J0909-0658	1998 Dec 22	Keck II	150	4.81	355.5–1125.1	600
DENIS-P J1023-1336	1998 Dec 22	KPNO	730	4.20	533.9–959.7	1800
DENIS-P J1024-0719	1998 Dec 24	KPNO	400	5.45	578.0–1069.0	1800
DENIS-P J1047-1815	1998 Dec 21	Keck II	900	0.84	631.2–804.0	3600
	1998 Dec 22	KPNO	730	4.20	533.9–959.7	1800
DENIS-P J1058-1548	1998 Dec 22	Keck II	150	4.81	355.5–1125.1	600
DENIS-P J1116-1945	1998 Dec 23	Keck II	150	4.81	355.5–1125.1	600
	1998 Dec 24	KPNO	400	5.45	578.0–1069.0	3600
DENIS-P J1158-1201	1998 Dec 24	KPNO	400	5.45	578.0–1069.0	1800
DENIS-P J1159+0057	1998 Dec 21	Keck II	900	0.84	631.2–804.0	1800
	1998 Dec 22	KPNO	730	4.20	533.9–959.7	1800
DENIS-P J1208+0149	1998 Dec 23	Keck II	150	4.81	355.5–1125.1	1200
	1998 Dec 24	KPNO	400	5.45	578.0–1069.0	1800
DENIS-P J1228-1547	1998 Dec 22	Keck II	150	4.81	355.5–1125.1	600
DENIS-P J1323-1806	1998 Dec 22	Keck II	150	4.81	355.5–1125.1	1600
DENIS-P J1431-1953	1998 Dec 23	Keck II	150	4.81	355.5–1125.1	600
DENIS-P J1441-0945	1998 Dec 21	Keck II	900	0.84	631.2–804.0	1300
	1998 Dec 23	Keck II	150	4.81	355.5–1125.1	600
EROS-MP J0032-4405	1998 Dec 23	Keck II	150	4.81	355.5–1125.1	2000
G 196-3 B	1998 Dec 23	Keck II	150	4.81	355.5–1125.1	900
Kelu 1	1998 Dec 22	Keck II	150	4.81	355.5–1125.1	400
LHS 102 A	1998 Dec 22	Keck II	150	4.81	355.5–1125.1	120
LHS 102 B	1998 Dec 22	Keck II	150	4.81	355.5–1125.1	900
LHS 1443	1998 Dec 22	Keck II	150	4.81	355.5–1125.1	600
LHS 2065	1998 Dec 22	Keck II	150	4.81	355.5–1125.1	300
	1998 Dec 23	KPNO	730	4.20	533.9–959.7	200
LHS 2243	1998 Dec 24	KPNO	400	4.20	533.9–959.7	600
LHS 2397b	1998 Dec 23	Keck II	150	4.81	355.5–1125.1	360
LHS 2924	1998 Jun 17	Keck II	300	4.87	365.2–865.3	300
LP 759-35	1998 Jun 17	Keck II	1200	1.26	653.2–782.8	300
2MASSW J0030+3139	1999 Jul 7	Keck II	150	4.81	355.5–1125.1	1600
2MASSs J0850+1057	1998 Dec 23	Keck II	150	4.81	355.5–1125.1	1200
2MASSW J1632+1904	1999 Jul 7	Keck II	150	4.81	355.5–1125.1	1600
VB10	1999 Jul 7	Keck II	150	4.81	355.5–1125.1	480

Table 3. Integration Limits of Spectral Ratios

Name	Numerator (nm)	Denominator (nm)	Feature
PC3	823.0–827.0	754.0–758.0	Pseudo-continuum
PC6	909.0–913.0	650.0–654.0	Pseudo-continuum
CrH1	856.0–860.0	861.0–865.0	CrH λ861.1
CrH2	984.0–988.0	997.0–1001.0	CrH λ996.9
FeH1	856.0–860.0	868.5–872.5	FeH λ869.2
FeH2	984.0–988.0	990.0–994.0	FeH λ989.6
H_2O1	919.0–923.0	928.0–932.0	H_2O λ930.0
TiO1	700.0–704.0	706.0–710.0	TiO λ705.3
TiO2	838.0–842.0	844.0–848.0	TiO λ843.2
VO1	754.0–758.0	742.0–746.0	VO λ743.4
VO2	799.0–803.0	790.0–794.0	VO λ791.2

Table 4. Measurements of PC Spectral Ratios

Brief Name	SpT	PC3	PC6	Source	SpT
	(Previous)				(Adopted)
GJ 752 A	dM2.5	0.99		TW93	dM2.5
LHS 102 A	dM3.5	1.09	2.31	Keck	dM3.5
GJ 402	dM4	1.12	2.62	MRZ96	dM4
GJ 873	dM3.5	1.13	2.33	MRZ96	dM4
DENIS-P J0247-1055		1.18	3.45	Keck	dM4.5
GJ 51	dM5	1.26		KHM91	dM5
GJ 866 AB	dM5	1.27		KHM91	dM5
GJ 905	dM5	1.32	4.65	KPNO	dM5
		1.27	4.69	MRZ96	
G 208-44 AB	dM5.5	1.33	5.07	KHM91	dM5.5
GJ 65 A	dM5.5	1.36	5.41	KHM91	dM5.5
LHS 1443	dM6	1.38	6.30	Keck	dM5.5
GJ 406	dM6	1.51	8.27	KPNO	dM6
VB 8	dM7	1.52	8.38	KHM91	dM7
LHS 3003	dM7	1.54	8.79	KHM91	dM7
LHS 2632	dM7.5	1.59	9.67	KHM91	dM7
LHS 2645	dM7.5	1.62	10.14	KHM91	dM7
CTI 1156	dM7	1.68	10.73	KHM91	dM7
LHS 2243	dM8	1.68	12.18	KHM91	dM7.5
		1.71	11.21	KPNO	
DENIS-P J1116-1945		1.84	15.51	Keck	dM8
		1.81	13.85	KPNO	
LP 412-31	dM8	1.83	12.26	KHM91	dM8
		1.85	16.54	MRZ96	
VB 10	dM8	1.86	11.97	KHM91	dM8
		1.84	19.13	MRZ96	
		1.76	19.23	Keck	
DENIS-P J1158-1201		1.87	16.32	Keck	dM8
		1.90	22.02	KPNO	
BRI 1222-1221	dM9	1.94	13.35	KHM91	dM8.5
GJ 569 B	dM8.5	1.96	8.87	KHM91	dM8.5
LHS 2397a	dM8	1.91	11.40	KHM91	dM8.5
		2.04	18.95	Keck	
DENIS-P J1024-0719		2.02	19.14	KPNO	dM9
TVLM 86811	dM9	2.03	12.15	KHM91	dM9
LHS 2924	dM9	2.04	16.35	KHM91	dM9
DENIS-P J0243-5432		2.06	21.28	Keck	dM9
DENIS-P J1023-1336		2.09	19.66	KPNO	dM9
		2.0:	20:	KPNO	dM9
DENIS-P J1431-1953		2.11	20.79	Keck	dM9
CTI 0126	dM8.5	2.11	16.65	KHM91	dM9

Table 4—Continued

Brief Name	SpT	PC3	PC6	Source	SpT
TVLM 51346	dM8.5	2.12	14.60	KHM91	dM9
PC 0025+0447	dM9.5	2.12	23.46	MBZ99	bdM9
RG 0050.0	dM8	2.16	17.66	KHM91	dM9
LHS 2065	dM9	2.21	15.41	KHM91	dM9
		2.16	16.70	Keck	
		2.29	17.63	KPNO	
DENIS-P J1208+0149		2.26	19.52	Keck	dM9.5
		2.7:		KPNO	
BRI 0021-0214	dM9.5	2.53	17.24	KHM91	dM9.5
		2.30	15.17	MRZ96	
		2.37	16.46	Keck	
		2.63	18.90	KPNO	
EROS-MP J0032-4405		2.45	18.35	Keck	bdL0
DENIS-P J1323-1806		2.59	19.51	Keck	dL0
DENIS-P J0909-0658		2.60	17.84	Keck	dL0
DENIS-P J1159+0057		2.64	17.69	KPNO	dL0
DENIS-P J1441-0945		2.71	18.25	Keck	dL1
G 196-3 B		2.71	17.24	Keck	bdL1
2MASSW J0030+3139	dL2	2.85	14.15	Keck	dL2
Kelu 1	dL2	2.87	16.36	Keck	bdL2
DENIS-P J1058-1548	dL3	3.08	15.45	Keck	dL2.5
DENIS-P J1047-1815		3.18	17.89	KPNO	dL2.5
LHS 102 B		6.07	15.95	Keck	dL4
DENIS-P J1228-1547	dL5	6.56	17.21	Keck	bdL4.5
DENIS-P J0205-1159	dL7	8.68	32.22	Keck	dL5
2MASSs J0850+1057	dL6	8.79	27.44	Keck	bdL5
2MASSW J1632+1904	dL8	12.05	82.70	Keck	bdL6
DENIS-P J0255-4700		13.51	60.08	Keck	dL6

References. — Acronyms: KHM91 = Kirkpatrick, Henry & McCarthy 1991; MRZ96 = Martín, Rebolo & Zapatero Osorio 1996; MBZ99 = Martín, Basri & Zapatero Osorio 1999; TW93 = Torres-Dodgen & Weaver 1993.

Note. — A colon indicates uncertain measurements due to low S/N ratio.

Table 5. Spectral Type – T_{eff}

Object	SpT	I-J	I-K	T_{eff} (K)	Reference
VB10	dM8	2.91	4.05	2700,2200	S96,JT97
LHS 2924	dM9	3.23	4.47	2400,2100	B99,JT97
LHS 2065	dM9	3.22	4.50	2300	LAH98
BRI 0021-0214	dM9.5	3.30	4.53	2300	LAH98
DENIS-P J0909-0658	dL0	3.20	4.70	2200	B99
EROS-MP J0032-4405	bdL0.5	3.70	4.92	1900	G99
Kelu 1	bdL2	3.50	5.00	2000,1900	B99,RLA97
DENIS-P J1058-1548	dL2.5	3.61	5.19	1900	B99
LHS 102 B	dL4	3.70	5.60	1800,1700	B99,G99
DENIS-P J1228-1547	bdL4.5	3.81	5.43	1800	B99
DENIS-P J0205-1159	dL5	3.82	5.28	1700,1800	B99,TK99
DENIS-P J0255-4700	dL6	3.66	5.28	1600	B99

References. — The quoted T_{eff} values come from: B99 = Basri et al. 1999; G99 = Goldman et al. 1999; JT97 = Jones & Tsuji 1997; LAH98 = Leggett, Allard & Hauschildt 1998; RLA97 = Ruiz, Leggett & Allard 1997; S96: Schweitzer et al. 1996; TK99=Tokunaga & Kobayashi 1999. The photometric data was taken from Bessell (1991), and LAH98.

Table 6. Molecular Band Spectral Ratios

Brief Name	CrH1	CrH2	FeH1	FeH2	H_2O1	TiO1	TiO2	VO1	VO2	Source
GJ 752 A	1.01		1.08			1.20	1.06	1.06	1.07	TW93
LHS 102 A	0.93	0.99	0.98	0.92	1.16	1.28	1.09	1.02	1.11	Keck
GJ 402	0.98		0.99	1.08	1.05	1.37	1.12	1.11	1.14	MRZ96
GJ 873	1.00	1.13	1.03	1.14	0.93	1.25	1.08	1.09	1.12	MRZ96
DENIS-P J0247-1055	0.80	0.58	0.94	0.87	0.74	1.55	0.78	1.11	1.11	Keck
s81292	0.99		1.02			1.23	1.06	1.09	1.11	SC92
GJ 51	0.97		1.01			1.55	1.28	1.13	1.21	KHM91
GJ 866 AB	0.96		1.00			1.64	1.38	1.17	1.23	KHM91
GJ 905	0.94	1.06	0.92	1.13	1.10	1.58	1.28	1.19	1.22	KPNO
	0.95		0.92	1.12	0.98	1.67	1.29	1.17	1.22	MRZ96
G 208-44 AB	0.96		0.95	1.15		1.41	1.29	1.15	1.28	KHM91
GJ 65 A	0.97		0.99			1.66	1.31	1.19	1.26	KHM91
LHS 1443	0.92	1.10	0.92	1.05	1.20	1.97	1.42	1.11	1.30	Keck
GJ 406	0.96	1.15	0.95	1.25	1.18	2.09	1.48	1.27	1.32	KPNO
VB 8	0.98		1.02			2.16	1.60	1.25	1.37	KHM91
LHS 3003	0.97		0.98			2.17	1.63	1.27	1.32	KHM91
LHS 2632	0.93		0.90			2.03	1.57	1.28	1.33	KHM91
LHS 2645	0.98		0.99			2.29	1.57	1.26	1.45	KHM91
LHS 2243	0.97		0.94			2.16	1.65	1.33	1.36	KHM91
	0.93	1.29	0.92	1.31	1.17	1.95	1.61	1.31	1.29	KPNO
CTI 1156	0.98		1.02			1.86	1.56	1.23	1.33	KHM91
DENIS-P J1116-1945	0.98	1.17	0.97	1.27	1.20	2.17	1.70	1.24	1.32	Keck
	0.98	1.63	0.99	1.82	1.80	2.09	1.64	1.21	1.26	KPNO
LP 412-31	1.03		1.05			2.34	1.82	1.34	1.39	KHM91
	1.04		1.06	1.77	1.07	2.34	1.79	1.33	1.36	MRZ96
VB 10	1.02		0.99			1.53	1.66	1.24	1.32	KHM91
	0.96	1.08	0.93	1.46	1.21	2.00	1.83	1.35	1.33	Keck
DENIS-P J1158-1201	0.99	1.20	1.01	1.33	1.20	2.35	1.72	1.19	1.40	Keck
	0.98	1.29	0.91	1.06	1.19	2.4:	1.64	1.51	1.71	KPNO
BRI 1222-1221	1.03		1.02			1.79	1.72	1.38	1.20	KHM91
GJ 569 B	1.00		1.01			1.37	1.69	1.16	1.32	KHM91
LHS 2397a	1.06		1.12			2.08	1.83	1.25	1.41	KHM91
	1.04	1.29	1.06	1.48	1.17	2.05	1.77	1.23	1.35	Keck
DENIS-P J1024-0719	0.99	1.39	0.89	1.30	1.44	2.08	1.39	1.50	1.21	KPNO
TVLM 86811	1.06		1.09			1.87	1.72	1.34	1.30	KHM91
LHS 2924	0.94		1.00			1.42	1.65	1.41	1.18	KHM91
DENIS-P J0243-5432	0.96	1.04	0.89	1.08	1.62	1.93	1.70	1.39	1.59	Keck
DENIS-P J1023-1336	0.97	1.31	0.98	1.37	1.27	1.87	1.86	1.21	1.35	Keck
DENIS-P J1431-1953	1.00	1.26	1.01	1.39	1.22	2.21	1.92	1.25	1.46	Keck
CTI 0126	0.98		1.03			1.87	1.56	1.23	1.34	KHM91
TVLM 51346	1.07		1.06			1.68	1.86	1.29	1.29	KHM91
PC 0025+0447	1.04	1.26	1.02	1.25	1.98	1.40	1.73	1.67		MBZ99

Table 6—Continued

Brief Name	CrH1	CrH2	FeH1	FeH2	H_2O1	TiO1	TiO2	VO1	VO2	Source
RG 0050.0	1.01		1.00			1.60	1.88	1.30	1.31	KHM91
LHS 2065	1.04		1.01			1.50	1.75	1.35	1.21	KHM91
	1.02	1.31	1.00	1.42	1.22	1.60	1.73	1.27	1.26	Keck
	1.02	1.40	1.01	1.60	1.22	1.67	1.72	1.39	1.24	KPNO
DENIS-P J1208+0149	1.01	1.20	0.98	1.32	1.19	1.77	1.80	1.21	1.31	Keck
	0.94	1.48	1.04	1.82	1.17	1.64	1.82	1.35	1.24	KPNO
BRI 0021-0214	1.10		1.18			1.13	1.57	1.09	1.21	KHM91
	1.17	1.85	1.20	1.92	1.62	1.16	1.51	1.21	1.22	MRZ96
	1.20	1.57	1.29	1.73	1.18	1.24	1.61	1.13	1.23	Keck
	1.17	1.34	1.22	1.58	1.14	1.26	1.59	1.20	1.26	KPNO
EROS-MP J0032-4405	1.04	1.30	1.08	1.37	1.48	1.08	1.32	1.24	1.27	Keck
DENIS-P J1323-1806	1.27	1.41	1.31	1.35	1.18	1.04	1.58	1.09	1.24	Keck
DENIS-P J0909-0658	1.13	1.38	1.25	1.45	1.20	1.06	1.46	1.13	1.18	Keck
DENIS-P J1159+0057	1.16	1.50	1.20	1.64	1.22	1.25	1.66	1.21	1.34	KPNO
DENIS-P J1441-0945	1.19	1.40	1.32	1.59	1.17	0.99	1.37	1.05	1.19	Keck
G 196-3 B	1.27	1.17	1.35	1.21	1.19	0.82	1.03	0.97	1.14	Keck
Kelu 1	1.35	1.46	1.49	1.58	1.18	0.84	1.17	0.90	1.20	Keck
DENIS-P J1058-1548	1.54	1.57	1.59	1.71	1.10	0.82	1.17	0.84	1.22	Keck
DENIS-P J1047-1815	1.34	1.56	1.50	1.81	1.24	1.01	1.44	1.04	1.33	KPNO
LHS 102 B	1.83	1.33	1.69	1.24	1.29	0.91	0.89	0.56	1.90	Keck
DENIS-P J1228-1547	1.76	1.46	1.71	1.46	1.13	0.84	1.05	0.53	1.49	Keck
DENIS-P J0205-1159	1.37	1.26	1.27	1.43	1.38	0.81	0.88	0.59	1.90	Keck
2MASSs J0850+1057	1.51	1.19	1.44	1.10	1.18	0.91	0.96	0.51	1.59	Keck
2MASSW J1632+1904	1.19	1.01	1.01	0.97	1.05	0.92	0.91	0.48	1.70	Keck
DENIS-P J0255-4700	1.19	1.11	1.07	1.03	1.36	0.88	0.86	0.49	1.94	Keck

Note. — Acronyms and symbols are the same as in Table 4.

Table 7. Pseudo-equivalent Width Measurements

Object	SpT	H_α	Li I	Na I	Cs I	Cs I*
LHS 1443	dM6	>-1.0	<0.5	9.8±0.3	<1.0	
DENIS-P J1116-1945	dM8	-2.1±0.6	<1.5	8.0±0.5	<1.0	
DENIS-P J1158-1201	dM8	-3.3±0.6	<1.5	10.5±0.5	<1.0	
VB10	dM8	-2.2±0.3	<0.3	10.8±0.5	<1.0	
LHS 2397a	dM8.5	-11.9±0.5	<0.5	9.8±0.4	1.1±0.4	
DENIS-P J0243-5432	dM9	>-2.0	<1.5	8.0±0.5	<1.5	
DENIS-P J1431-1953	dM9	>-2.0	<2.0	9.7±0.5	<1.5	
LHS 2065	dM9	-14.5±0.5	<0.5	9.2±0.4	2.0±0.4	
DENIS-P J1208+0149	dM9	-1.0±0.5	<1.0	11.8±0.5	<1.5	
BRI 0021-0214	dM9.5	>-1.0	<0.5	7.0±0.5	1.8±0.4	
EROS-MP J0032-4405	bdM9.5	-1.7±0.7	3.3±0.7	5.8±0.6	5.0±0.5	
DENIS-P J1323-1806	dL0	-1.1±0.5	<1.0	6.0±0.5	2.6±0.5	
DENIS-P J0909-0658	dL0	-1.5±0.3	<0.5	7.5±0.5	2.1±0.4	0.81
DENIS-P J1441-0945	dL1	-2.1±0.6	<0.5	6.3±0.5	2.5±0.3	
G 196-3 B	bdL1	>-1.0	4.7±0.3	1.4±0.4	2.0:	1.75
Kelu 1	bdL2	>-1.0	0.6±0.3	3.1±0.4	3.0±0.4	2.17
DENIS-P J1058-1548	dL2.5	-1.0±0.4	<0.5	5.2±0.3	2.9±0.4	2.30
LHS 102 B	dL4	>-4.0	<2.5	2.8±0.6	6.4±0.5	3.70
DENIS-P J1228-1547	bdL4.5	>-1.0	3.2±0.4	3.5±0.4	4.8±0.4	4.22
2MASSs J0850+1057	bdL5	>-2.5	13.7±0.5	1.7±0.4	5.7±0.6	
DENIS-P J0205-1159	dL5	>-3.0	<2.0	<3.0	6.6±0.6	5.00
2MASSW J1632+1904	bdL6	>-5.0	7.0:	<2.5	5.6±1.0	
DENIS-P J0255-4700	dL6	>-2.0	<1.0	<1.2	6.3±0.5	6.14

*PEW of the Cs I 852.1 nm line measured in the high resolution spectra presented by Basri et al. (1999).

Note. — The PEW of Na I corresponds to the blend of the 818.3 and 819.5 nm doublet and it is affected by telluric absorption.

1

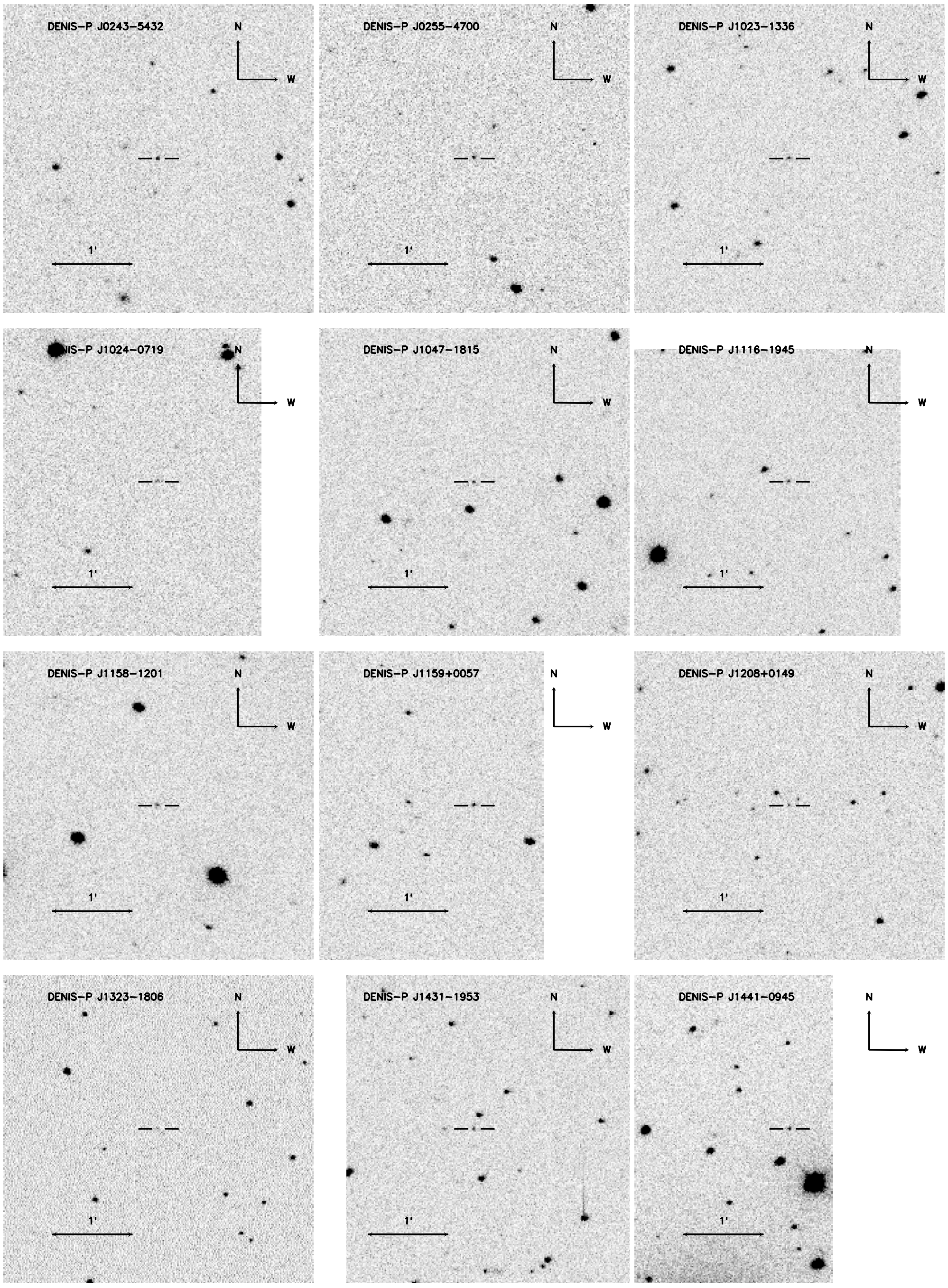

Fig. 1. Finding chart obtained with the I DENIS image. The size of this chart is $\sim 3.5' \times 3.5$. North is up and East is left

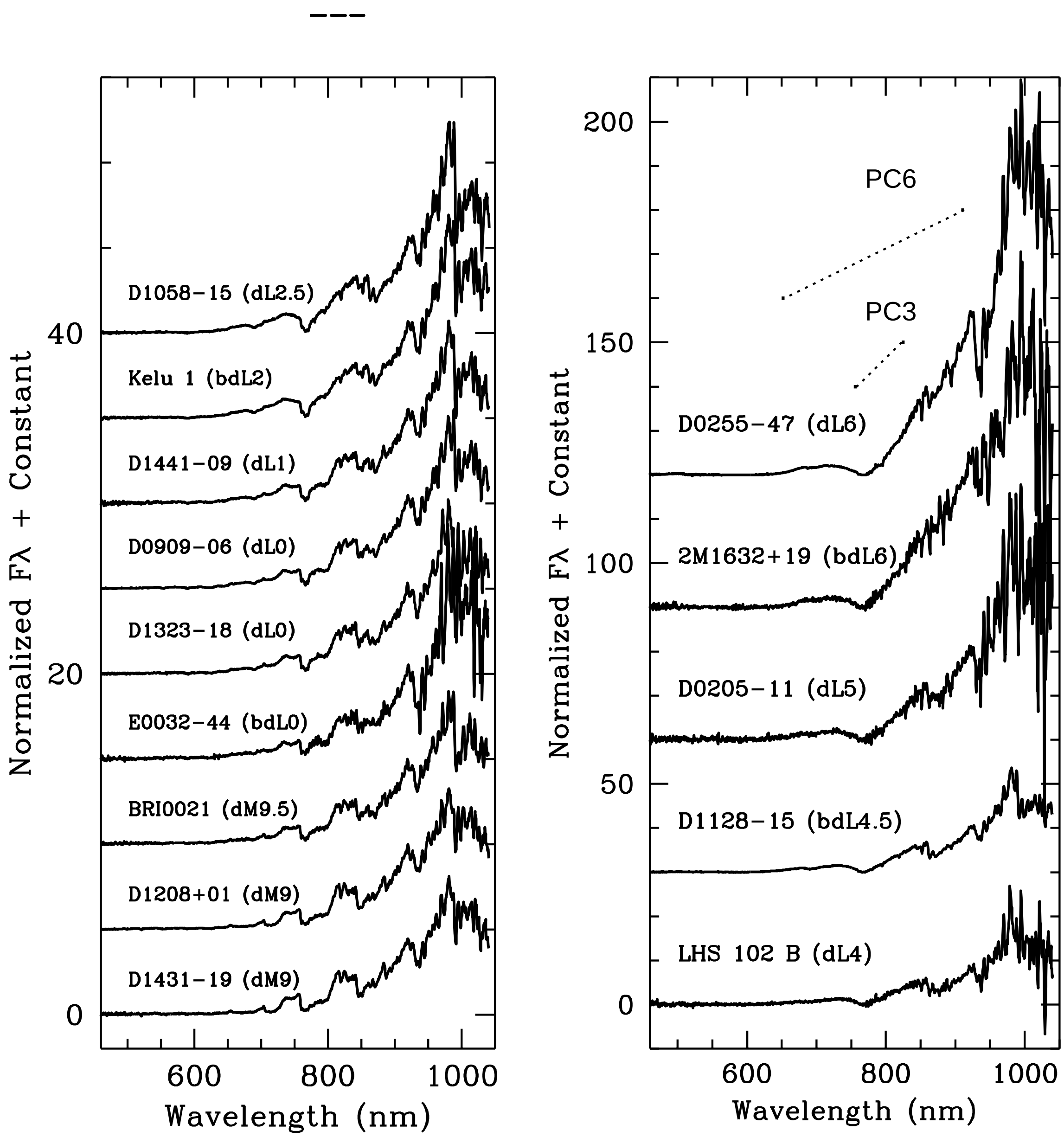
D1058-15 (dL2.5)
Kelu 1 (bdL2)
D1441-09 (dL1)
D0909-06 (dL0)
D1323-18 (dL0)
E0032-44 (bdL0)
BRI0021 (dM9.5)
D1208+01 (dM9)
D1431-19 (dM9)
Normalized Fλ + Constant
Wavelength (nm)
PC6
PC3
D0255-47 (dL6)
2M1632+19 (bdL6)
D0205-11 (dL5)
D1128-15 (bdL4.5)
LHS 102 B (dL4)

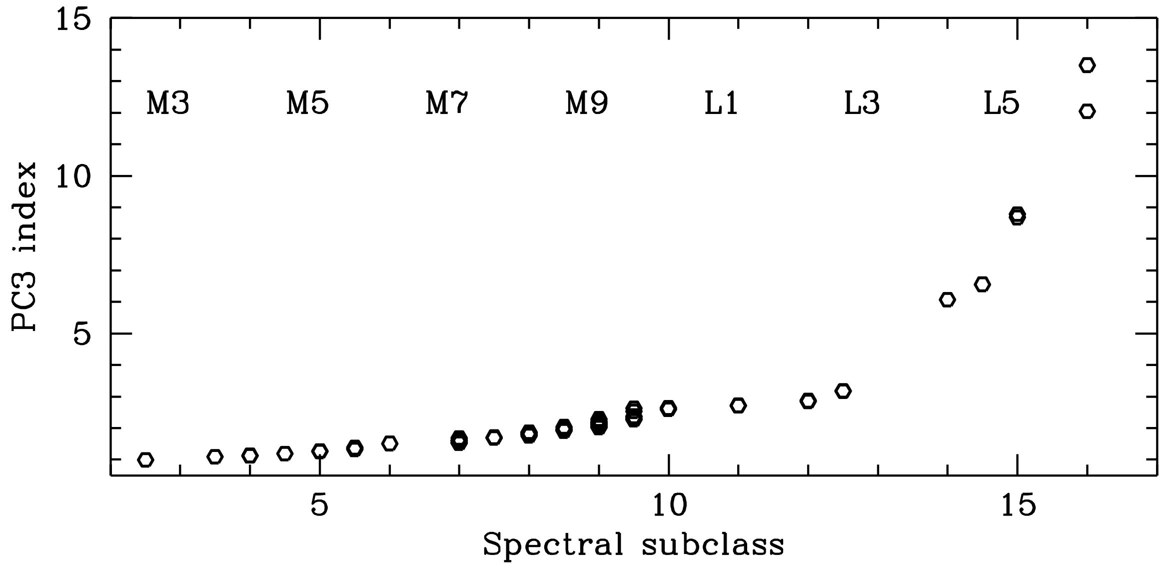

PC3 index
Spectral subclass
M3
M5
M7
M9
L1
L3
L5

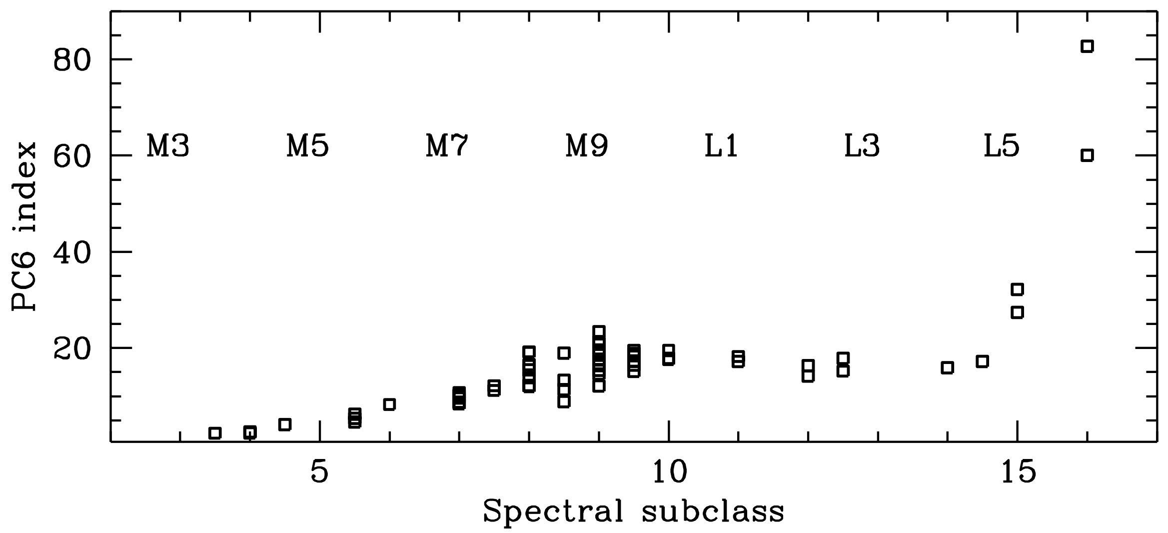

PC6 index
Spectral subclass
M3
M5
M7
M9
L1
L3
L5

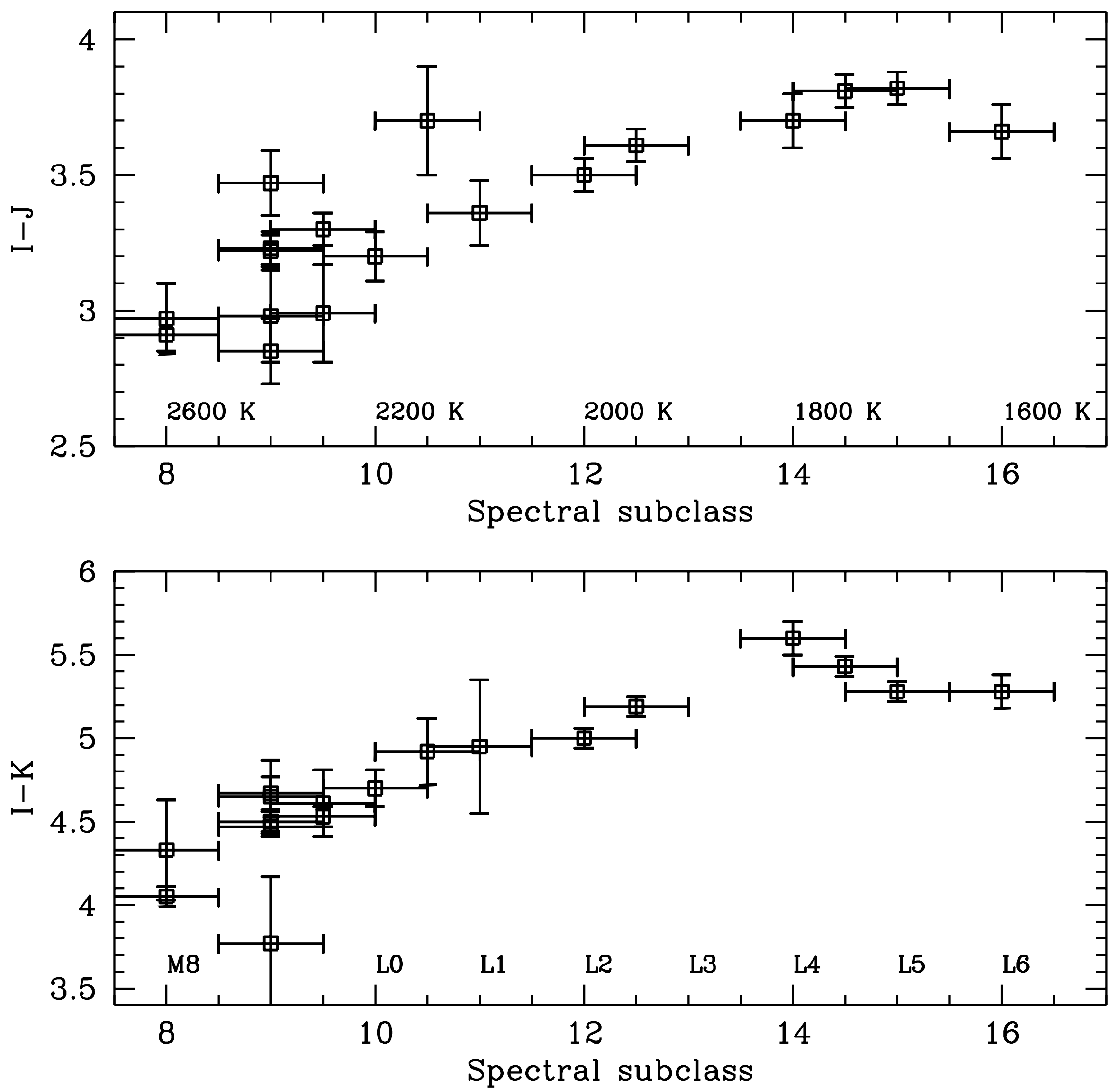
I−J
4
3.5
3
2.5
2600 K
2200 K
2000 K
1800 K
1600 K
8
10
12
14
16
Spectral subclass
I−K
6
5.5
5
4.5
4
3.5
M8
L0
L1
L2
L3
L4
L5
L6
Spectral subclass

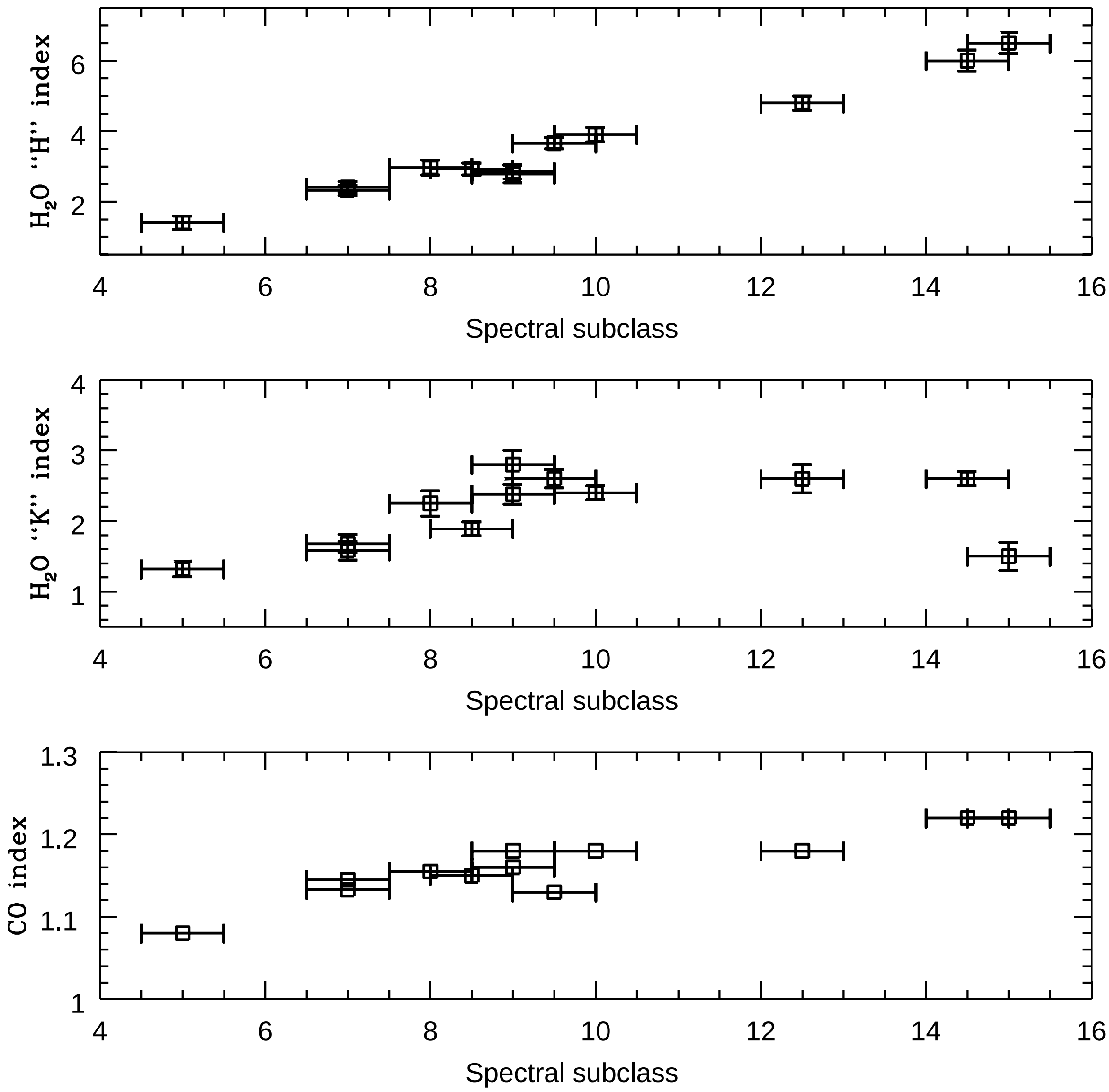
H2O "H" index
Spectral subclass
H2O "K" index
Spectral subclass
CO index
Spectral subclass

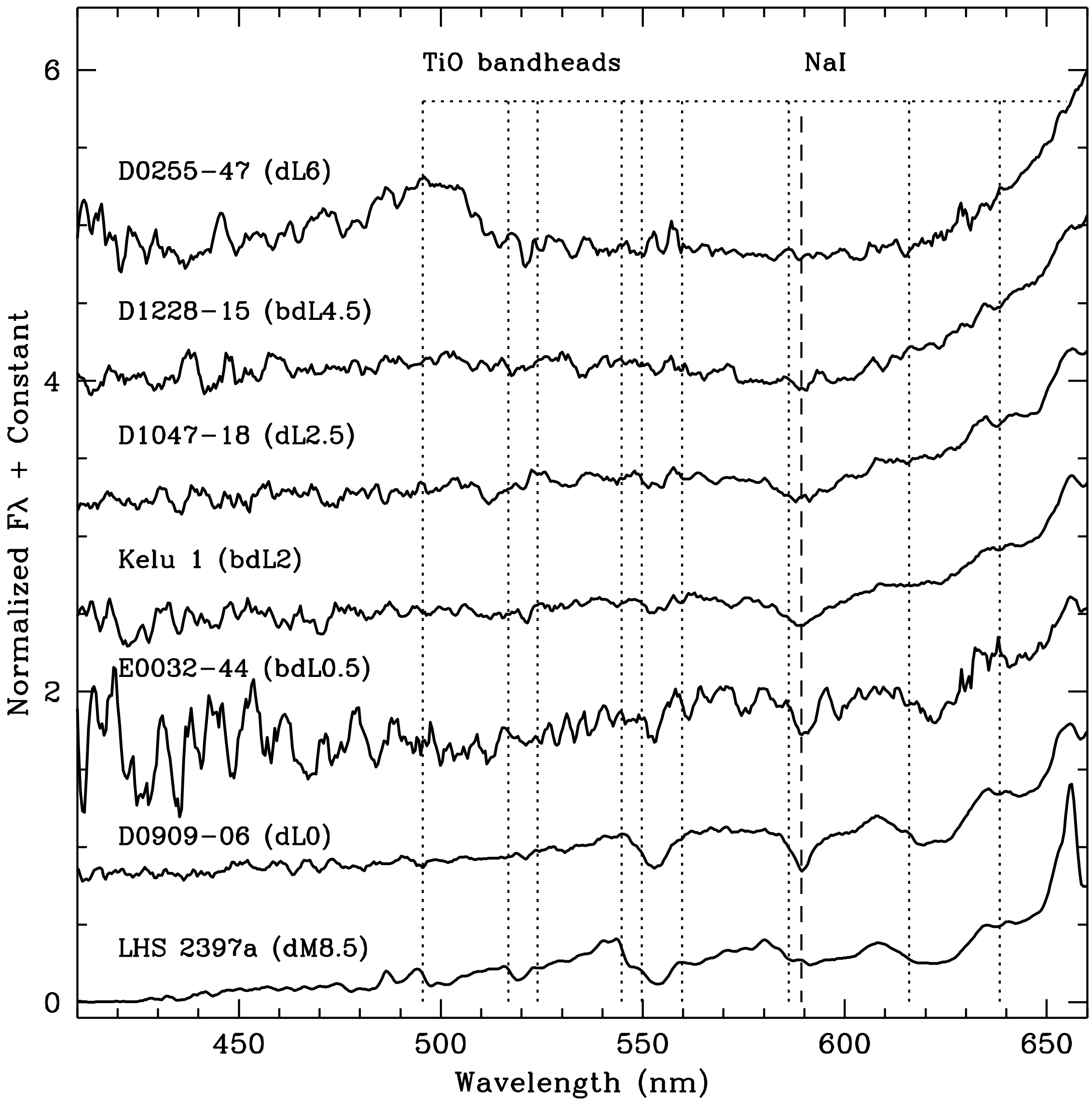
TiO bandheads
NaI
D0255−47 (dL6)
D1228−15 (bdL4.5)
D1047−18 (dL2.5)
Kelu 1 (bdL2)
E0032−44 (bdL0.5)
D0909−06 (dL0)
LHS 2397a (dM8.5)
Normalized Fλ + Constant
Wavelength (nm)
0
2
4
6
450
500
550
600
650

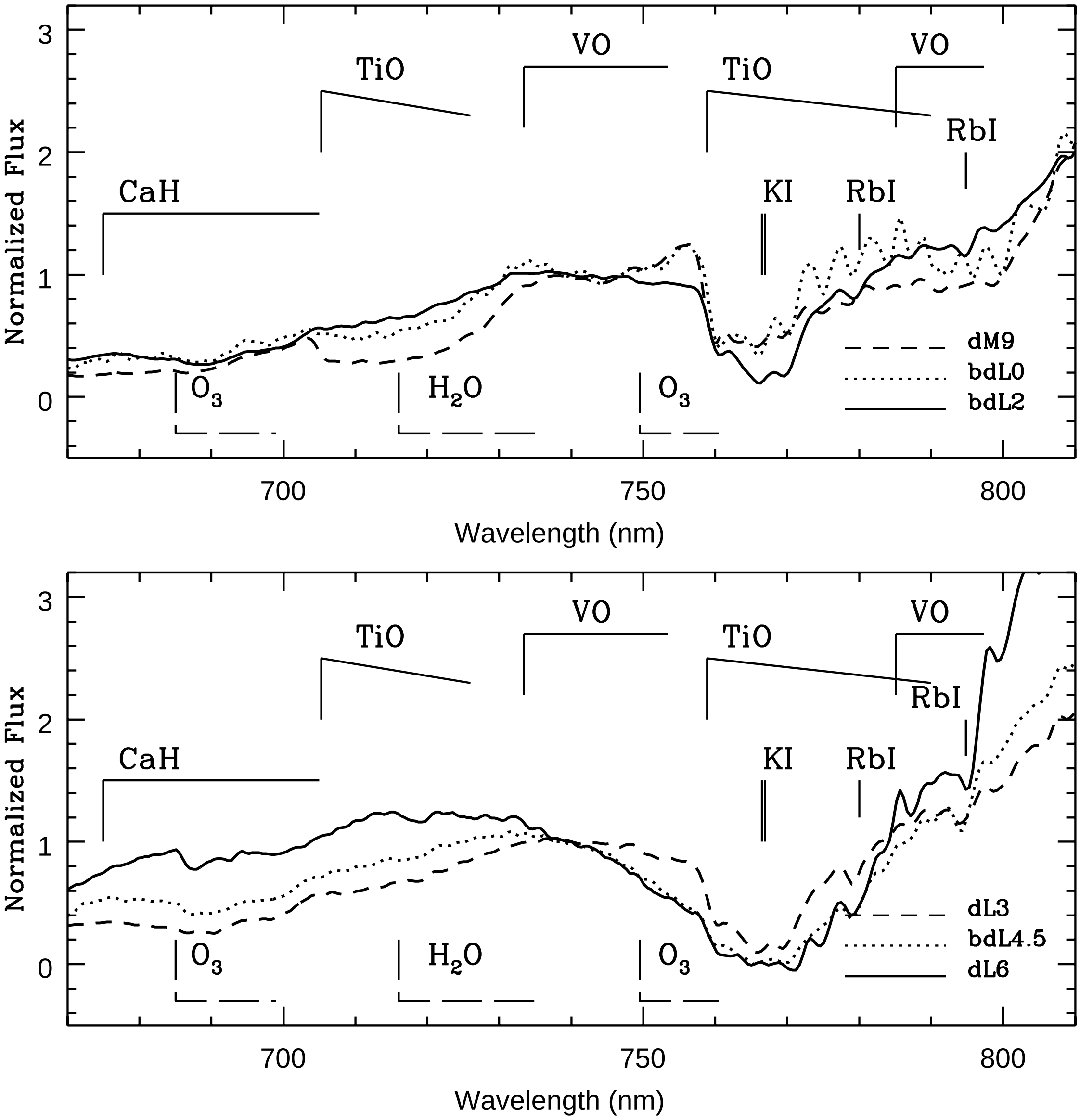
TiO
VO
TiO
VO
RbI
CaH
KI
RbI
O3
H2O
O3
dM9
bdL0
bdL2
Normalized Flux
Wavelength (nm)
TiO
VO
TiO
VO
RbI
CaH
KI
RbI
O3
H2O
O3
dL3
bdL4.5
dL6
Normalized Flux
Wavelength (nm)

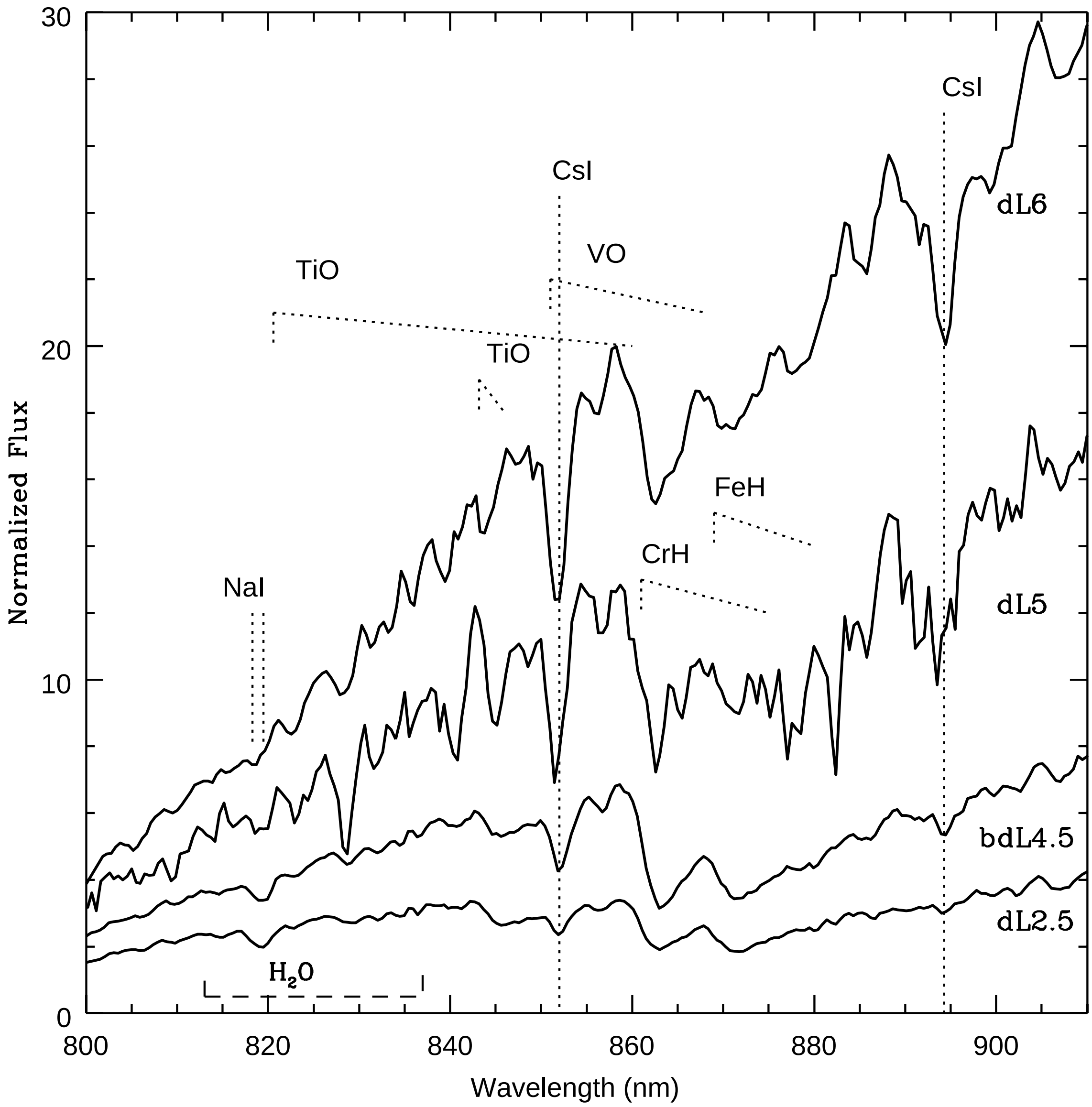
Normalized Flux
Wavelength (nm)
0
10
20
30
800
820
840
860
880
900
CsI
CsI
TiO
VO
TiO
FeH
CrH
NaI
dL6
dL5
bdL4.5
dL2.5
H_2O

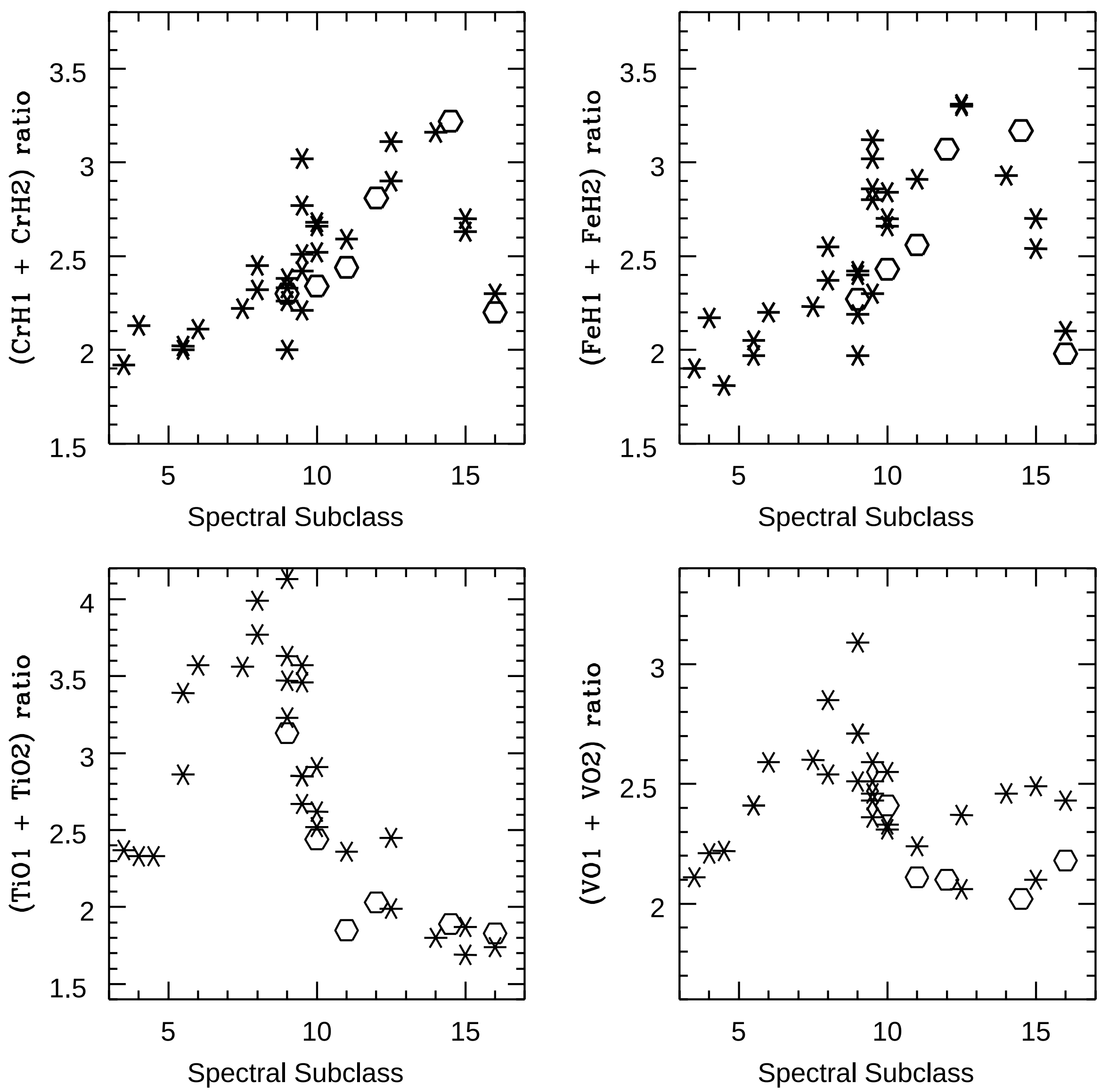
(CrH1 + CrH2) ratio
(FeH1 + FeH2) ratio
(TiO1 + TiO2) ratio
(VO1 + VO2) ratio
Spectral Subclass
Spectral Subclass
Spectral Subclass
Spectral Subclass

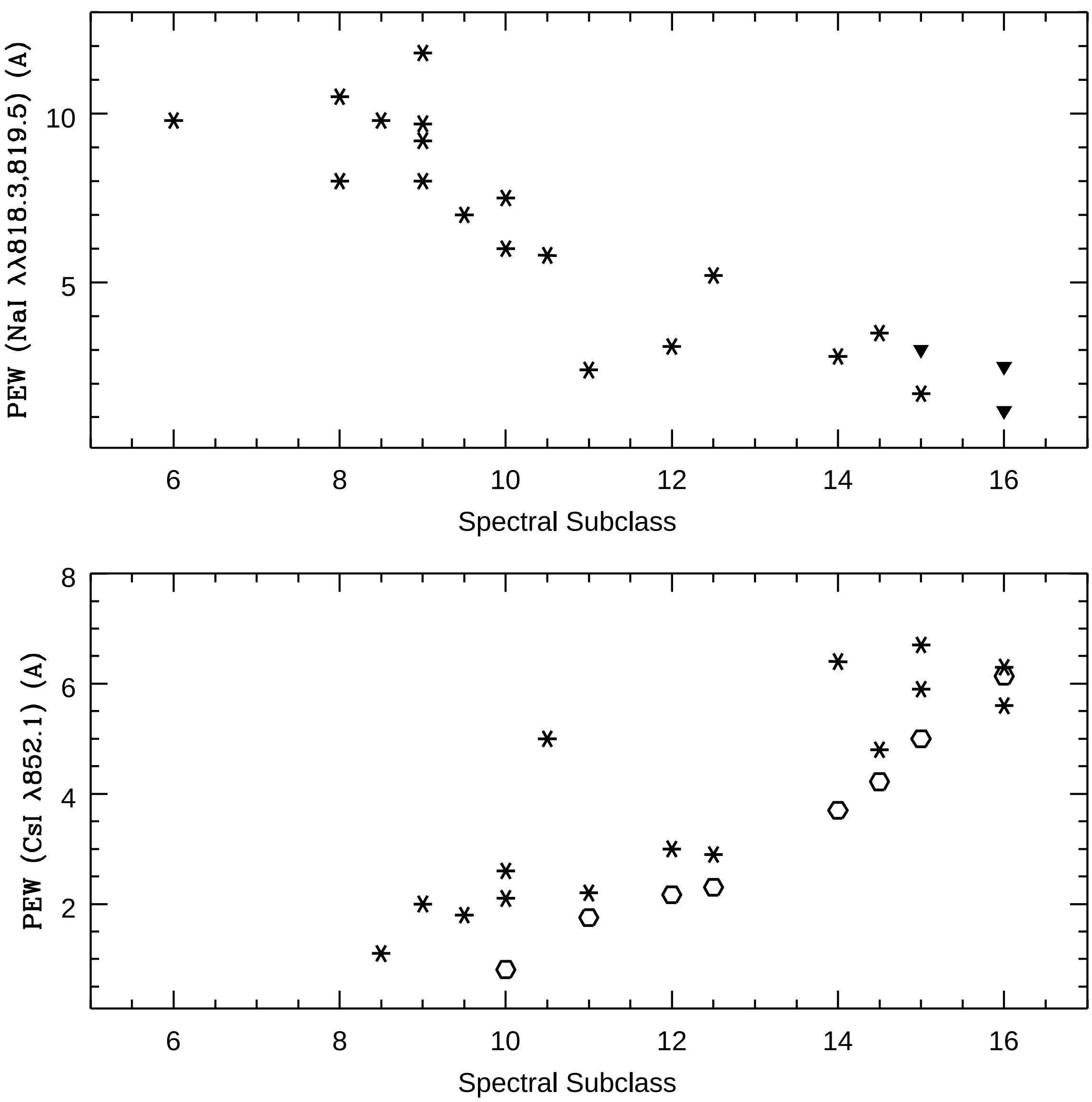
PEW (NaI λλ818.3,819.5) (A)
10
5
6
8
10
12
14
16
Spectral Subclass
PEW (CsI λ852.1) (A)
8
6
4
2
6
8
10
12
14
16
Spectral Subclass

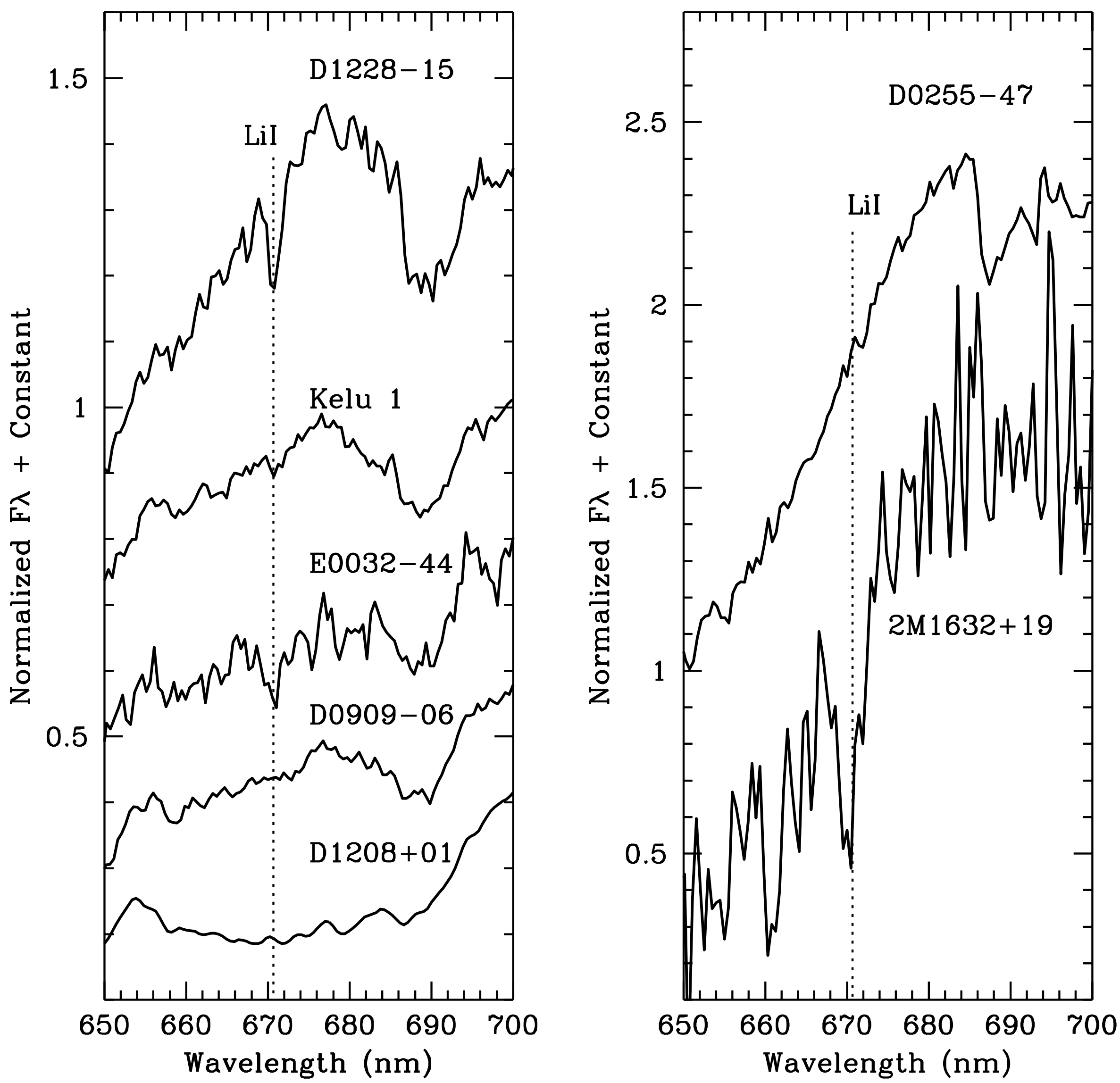
D1228−15
LiI
Kelu 1
E0032−44
D0909−06
D1208+01
Normalized Fλ + Constant
Wavelength (nm)
D0255−47
LiI
2M1632+19
Normalized Fλ + Constant
Wavelength (nm)

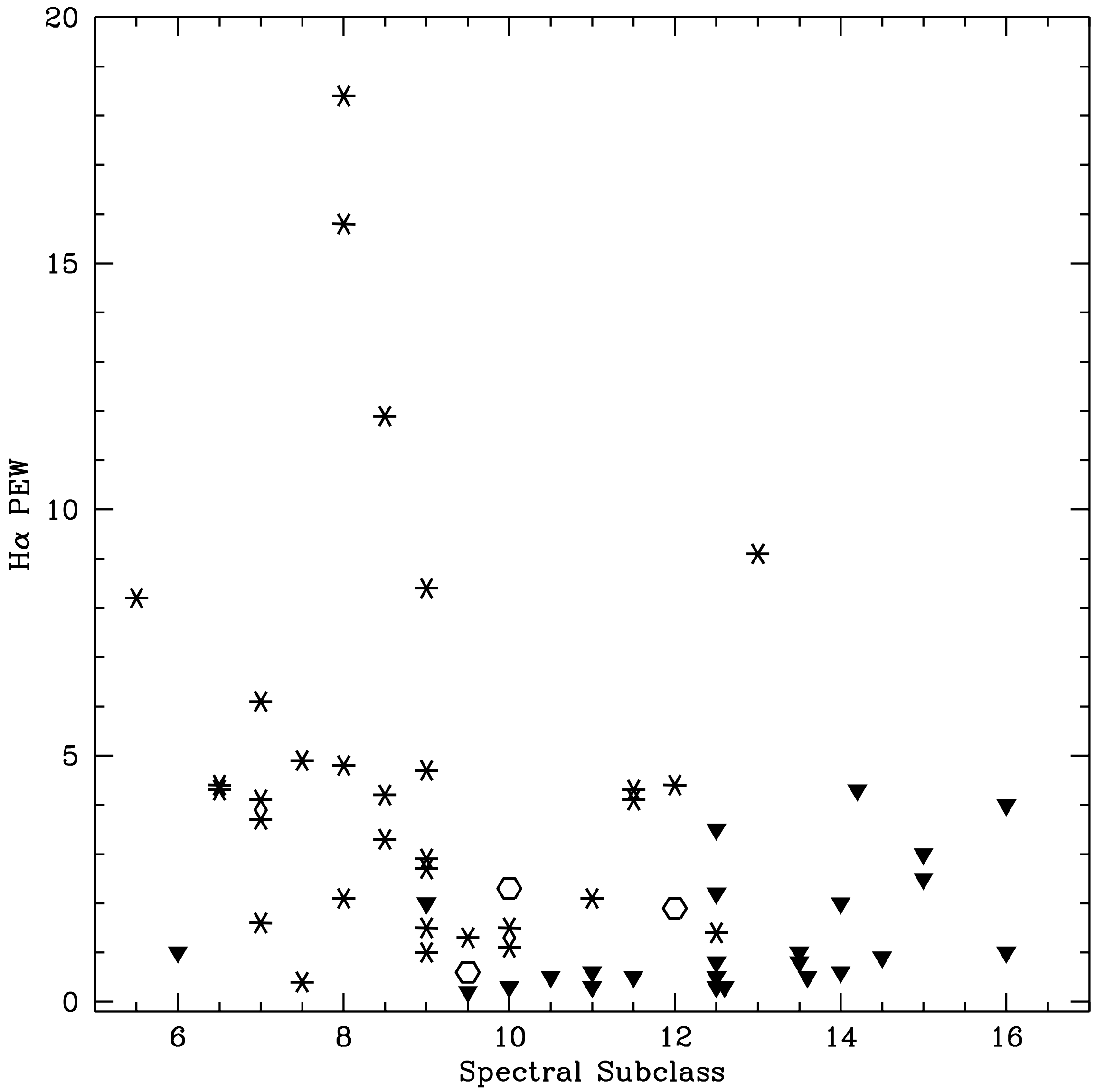
20
15
10
5
0
Hα PEW
6
8
10
12
14
16
Spectral Subclass

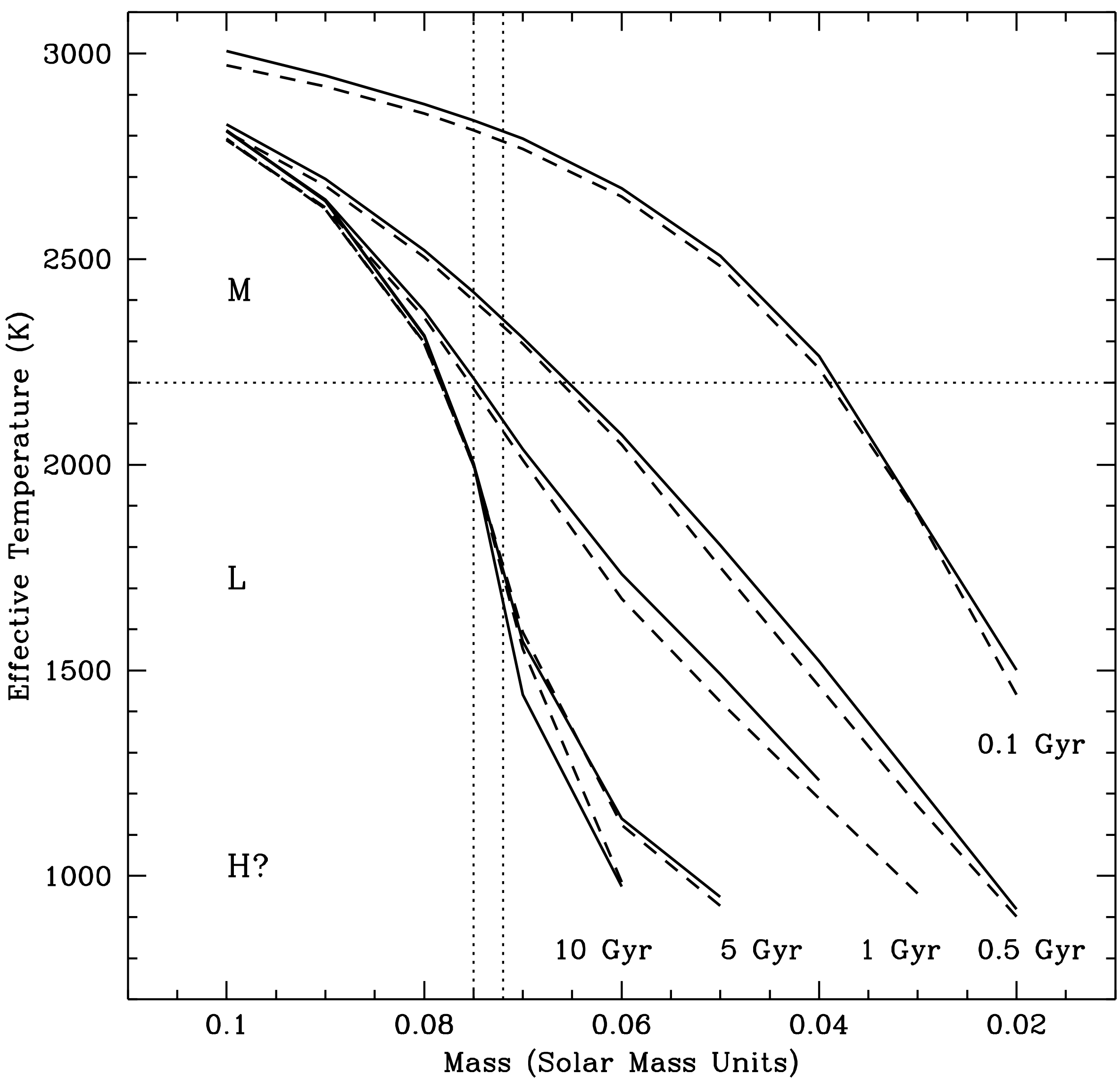
3000
2500
2000
1500
1000
Effective Temperature (K)
M
L
H?
0.1 Gyr
10 Gyr
5 Gyr
1 Gyr
0.5 Gyr
0.1
0.08
0.06
0.04
0.02
Mass (Solar Mass Units)

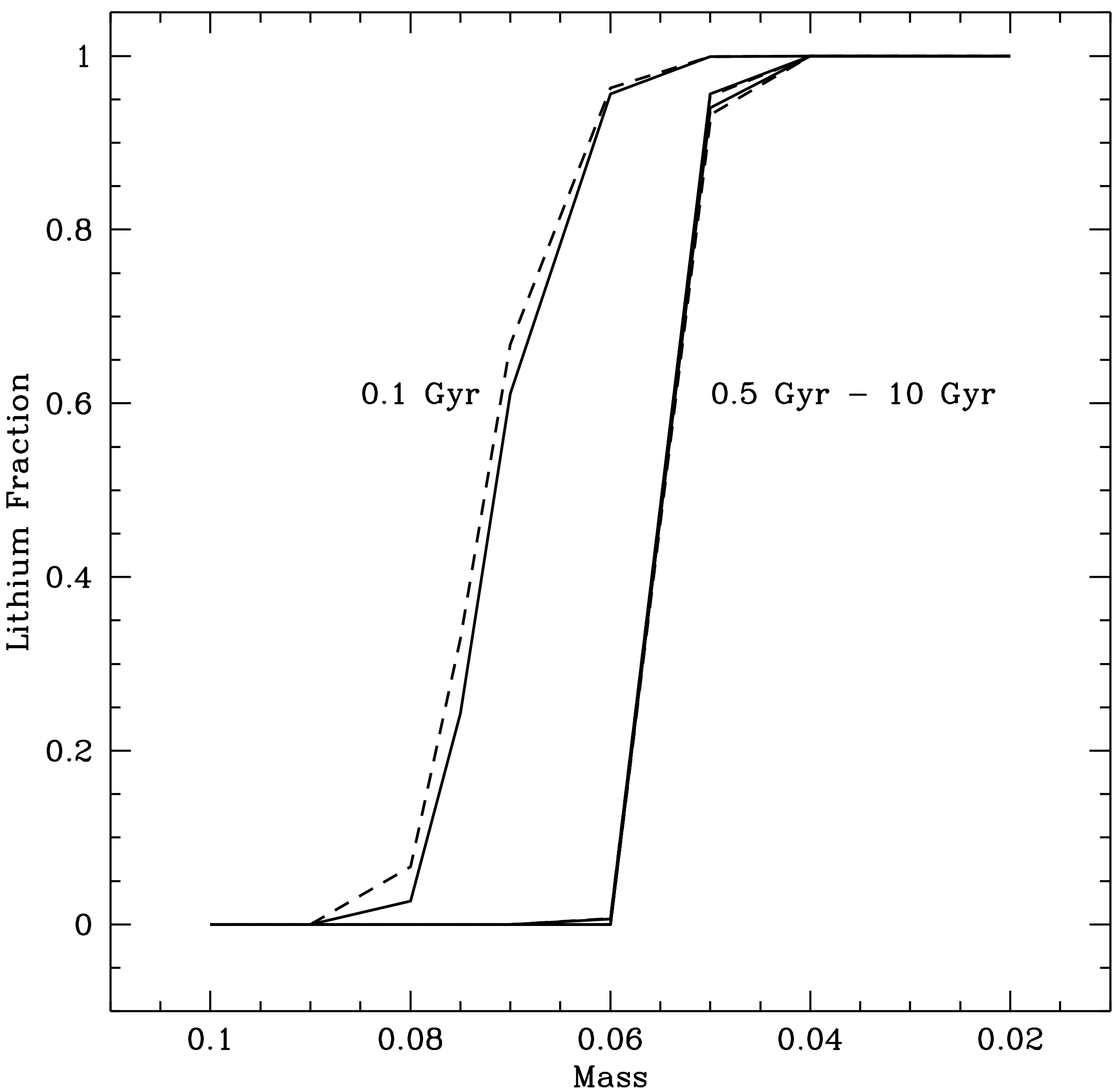

1
0.8
0.6
0.4
0.2
0
Lithium Fraction
0.1 Gyr
0.5 Gyr – 10 Gyr
0.1
0.08
0.06
0.04
0.02
Mass

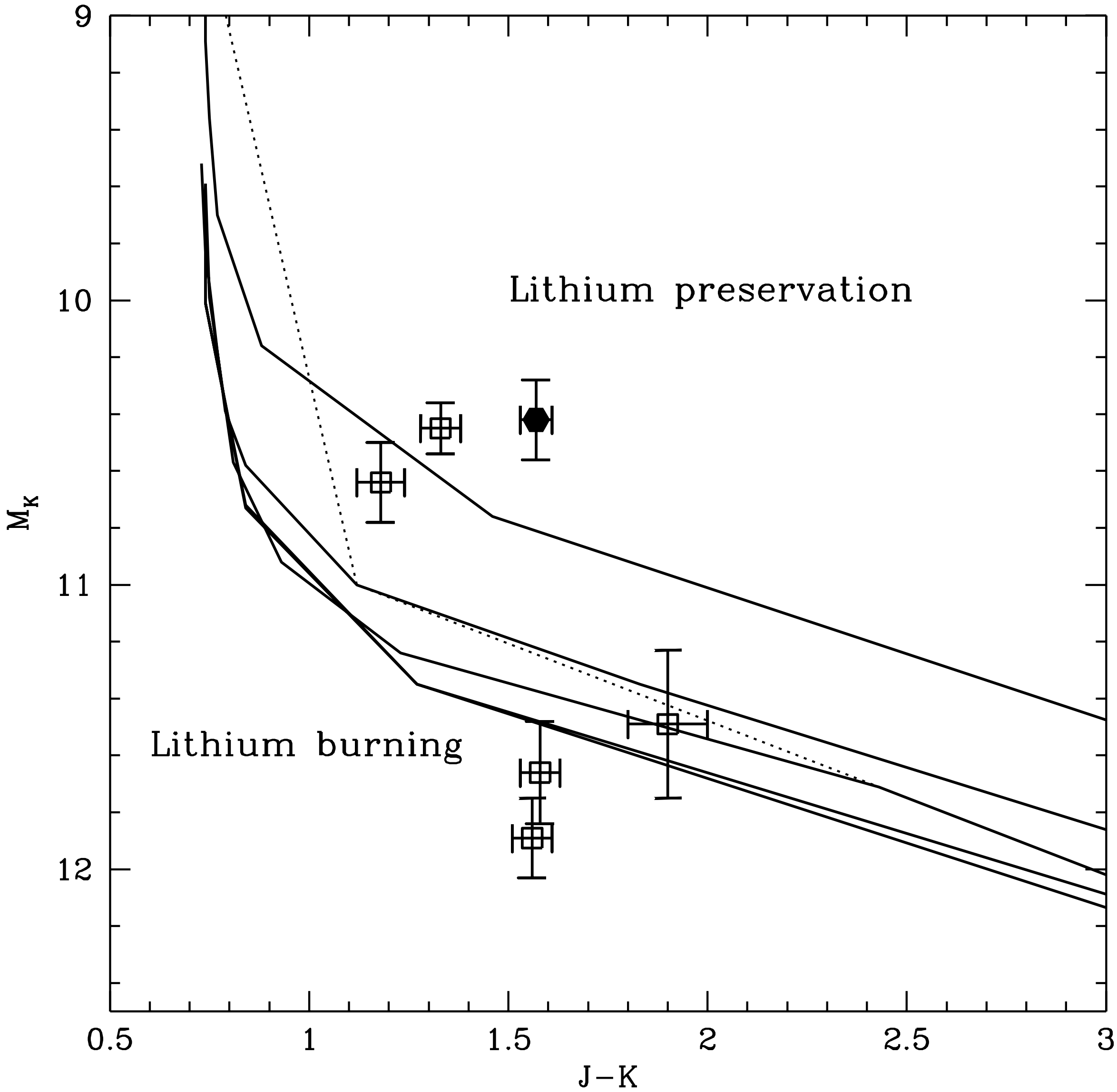
Lithium preservation
Lithium burning
M_K
J−K
9
10
11
12
0.5
1
1.5
2
2.5
3

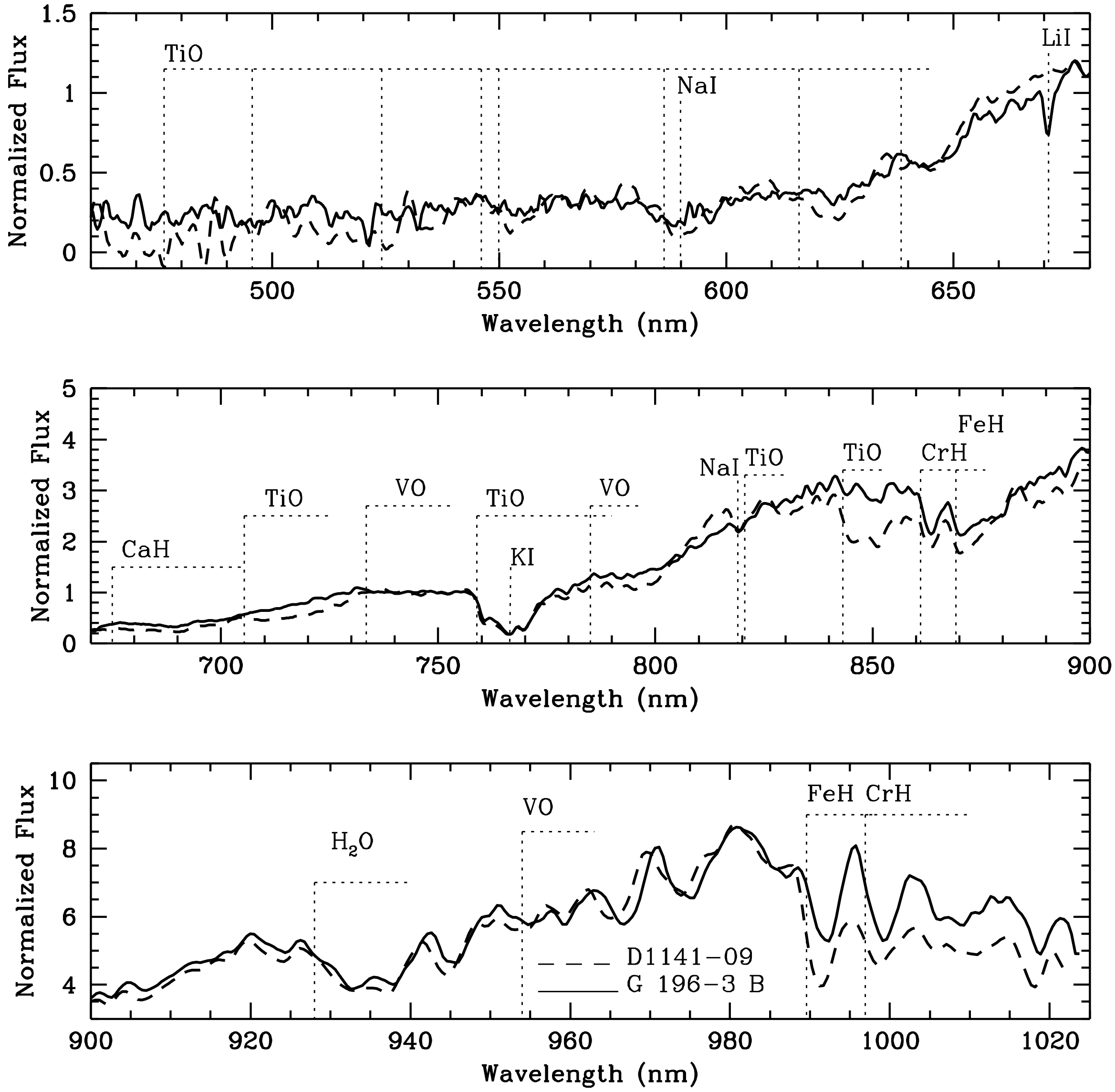
Normalized Flux
Wavelength (nm)
TiO
NaI
LiI
CaH
VO
KI
CrH
FeH
H2O
D1141-09
G 196-3 B